Fractional charges in conventional sequential electron tunneling

Roman-Pascal Riwar
JARA Institute for Quantum Information (PGI-11), Forschungszentrum Jülich, 52425 Jülich, Germany

(Received 28 November 2018; revised manuscript received 25 November 2019; published 16 December 2019)

The notion of fractional charges was up until now reserved for quasiparticle excitations emerging in strongly correlated quantum systems, such as Laughlin states in the fractional quantum Hall effect, Luttinger quasiparticles, or parafermions. Here, the author consider topological transitions in the full counting statistics of standard sequential electron tunneling and find that they lead to charge fractionalization—strikingly without requiring exotic quantum correlations. This conclusion relies on the realization that fundamental integer charge quantization fixes the global properties of the transport statistics, whereas fractional charges can only be well-defined locally. We then show that the reconciliation of these two contradicting notions results in a nontrivially quantized geometric phase defined in the detector space. In doing so, we show that detector degrees of freedom can be used to describe topological transitions in nonequilibrium open quantum systems. Moreover, the quantized geometric phase reveals a profound analogy between the fractional charge effect in sequential tunneling and the fractional Josephson effect in topological superconducting junctions, where likewise the Majorana- or parafermions exhibit a charge which is at odds with the Cooper pair charge as the underlying unit of the supercurrent. To provide means for an experimental verification of our claims, we discuss highly feasible transport models, such as weakly tunnel-coupled quantum dots or charge islands. We show that the geometric phase can be accessed through the detector's waiting-time distribution. Finally, we find that topological transitions in the transport statistics could even lead to new applications, such as the unexpected possibility to directly measure features beyond the resolution limit of a detector.

DOI: 10.1103/PhysRevB.100.245416

I. INTRODUCTION

The fundamental unit, in which transport is exchanged between electronic systems, is the elementary charge of the electron, e. However, in the solid state, strong quantum correlations and topological phase transitions are known to lead to the emergence of particles and excitations which appear to carry, due to their collective nature, a charge different from e. The probably best-known example is the doubly charged Cooper pair in superconductors. Notably, there can also appear excitations with a *fractional* charge, such as Laughlin quasiparticles in the fractional quantum Hall effect [1], electronic realizations of parafermions [2], and quasiparticles in Luttinger liquid nanowires [3–5]. Importantly, some of these exotic excitations might serve as building blocks for protected quantum computing [2,6], and transport properties in units of fractional charges are widely considered as smoking gun signatures of their existence [7–13].

However, ironically, the more precisely we strive to measure such fractional charges, the more we approach the limit of fundamental integer charge quantization, where any fractional charge should be completely obscured. Importantly, when considering the entire full-counting statistics (FCS), the transported charge *is* measured with arbitrary precision, since we include the cumulants of all orders. And indeed, it has been shown that the violation of integer charge quantization is visible in the FCS of Luttinger liquid theory, which consequently fails to reproduce a fully physical moment generating function [14]. Therefore, defining fractional charges by means of a field theory with a noninteger valued charge operator [3] does not suffice when considering the FCS. We believe that this calls for a proper understanding of the meaning of fractional charges in the context of transport statistics.

In this work, we consider the FCS in the simplest possible, classical transport regime of sequential electron tunneling [15]. Importantly, by taking into account the full system-detector dynamics, we come to the conclusion that fractional charges are by no means a unique property of systems with strong quantum correlations, and on the contrary can

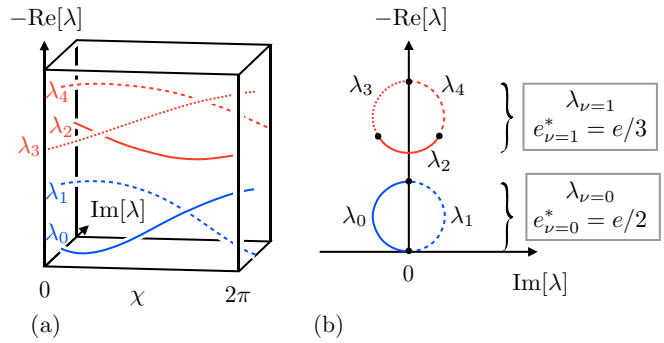

FIG. 1. (a) Generic spectrum of $W(\chi)$, describing the combined dynamics of system and detector (see Sec. II). There are two braid subblocks with broken periodicity. The lower one (blue) has a periodicity of 4π, and the upper one (red) a periodicity of 6π. (b) The same spectrum projected onto the complex plane. The black dots indicate the eigenvalues at $\chi = 0$. We see that the five eigenvalues merge into two bands, with the indices $\nu = 0$ and $\nu = 1$. As explained in Sec. II, we can assign the charges $e/2$ and $e/3$ to these two bands.

already occur on the level of conventional sequential tunneling through quantum dots or metallic islands. We show that here, the fractionalization is a consequence of a topological transition occurring in FCS of nonequilibrium transport, which can be described by the braid group [16,17], referred to as a braid phase transition. We show that each eigenmode of the detector dynamics contributes to the transport, in general, with an individual fractional charge; see Fig. 1. Namely, for a generic eigenspectrum, we find that we can map the FCS of ordinary electrons to an auxiliary system transporting fractionally charged quasiparticles, observed with a detector resolving only integer charges. Here, we thus interpret the elementary charge e as a fundamental *resolution limit* of the transport or charge detector. Of course, the quasiparticles appearing in our analogy are hypothetical, in the sense that the system is only physical once charge quantization is reestablished through the finite detector resolution. However, due to integer charge quantization being fundamental, we argue that from a charge transport perspective, they are just as hypothetical as quasiparticles in strongly correlated systems, to which one commonly assigns noninteger charge eigenvalues. This is the case for Luttinger liquids [3,14] or similarly chiral Luttinger liquids describing the edge state of the FQHE [18]. In particular, we find that the signatures in the transport statistics of ordinary sequential electron tunneling are topologically *indistinguishable* from those occurring in the transport statistics of quasiparticles in strongly correlated systems [7–14,19].

Importantly, our finding suggests that the numerous efforts and propositions to detect exotic quasiparticles via their fractional transport properties [7–13,19–21] may not be as conclusive as generally expected. On the upside, however, we show that one can realize topologically protected phases of fractional charges in condensed matter systems with very simple means of ordinary classical transport, avoiding difficulties related to controlling strongly correlated quantum systems. It is merely the mechanism for creating the fractional charges which is different, as in our case, all we need is a topological transition in a completely classical dynamics, where the maximal fractionalization depends simply on the number of available, local degrees of freedom.

We note that in some limiting cases, the emergence of fractional charges in sequential electron tunneling has already been noted; see, e.g., Refs. [15,22,23]. However, the deep connection to topological phase transitions in the detector dynamics, and thus the inherent protection of the fractional phases, has—to our best knowledge—been overlooked in the existing literature. Moreover, the authors of said literature, in general, made sure to refer to these charges as merely "effective" fractional charges, and they did not embark on a comparison to notions of fractional charges in strongly correlated systems. We aim to show in this paper that the topological considerations of the detector statistics allows for such a comparison. Furthermore, we note that in the context of the integer quantum Hall effect, it has been predicted that so-called "half-Levitons" can be generated even in the absence of strong correlations [24]. In that work it is, however, required that the flux induced by the injection voltage equals exactly π, leaving thus again the open question, how far the effect is protected. More recently, another work predicted an "almost" topologically protected fractional charge in a noninteracting quantum dot, when performing adiabatic pumping from a weak to strongly coupled dot [25] (where topological protection is lost due to nonadiabatic corrections). In our work, we require neither pumping nor strong coupling. Furthermore, Ref. [25] focuses on the average pumped current only, that is, the lowest cumulant, whereas we consider a definition of fractional charges requiring the entire FCS.

As a further main result, we show that the reconciliation of fractional charges and integer charge quantization leads to nontrivially quantized geometric phases emerging in the detector space. While geometric phases are known to give rise to topological numbers which describe many closed quantum systems [26,27], their generalization to open quantum systems is still an actively considered open problem [28–36]. We here contribute to this field, by proposing to describe topological transitions in open quantum systems through geometric phases defined along the detector degrees of freedom, which occur naturally, when coupling a quantum system to an environment. By relating the nontrivial quantization to the occurrence of fractional charges being at odds with integer charge quantization, we are furthermore able to assign a concrete physical meaning to the geometric phases.

Based on this result, we can show, in addition, that the fractional charge effect in sequential electron tunneling represents a classical analogy to the fractional Josephson effect emerging in topological superconducting junctions [37–43]. In the fractional Josephson effect, the transport is mediated by excitations with a fractional Cooper pair charge, such as the Majorana- or parafermions with a 4π [37–40], respectively, an 8π Josephson effect [41–43]. The analogy relies on the fact, that also here, the charge of the Majorana- and parafermions are at odds with the Cooper pair charge, giving thus rise to the very same nontrivially quantized geometric phases. In fact, we can think of the fractional transport of electrons as a classical simulation of the fractional Josephson effect. In a similar spirit, the simulation of topological features known from quantum coherent systems by means of a classical stochastic dynamics has been recently and prominently demonstrated in the diffusion of polymers [44,45], by exploiting the structural similarity between the Schrödinger equation and the diffusion equation. Likewise, the realization of a Su-Schrieffer-Heeger (SSH) model has been recently proposed using the full-counting statistics of single electron transistors [46]. We note that we have reason to believe that in our particular case, the simulation might actually be more stable than the original. The fractional Josephson effect is strongly susceptible to the breaking of fermion parity [37,47,48]. The topology of the incoherent transport, however, is *defined* in the single electron transport, and thus by nature stable with respect to parity breaking.

In the final part of our work, we aim to point towards experimental verifications of our claims and ouline potential applications. First, we study a regime, where a measurement of the lowest few cumulants of the current suffices to determine the fractional charge of the stationary mode. With the continued experimental progress in the detection of higher cumulants of the current [49–59] we believe that the fractional nature of sequential electron transport could be verified with existing technologies.

When going beyond this Poissonian regime, and when trying to measure fractional charges of the higher eigenmodes of the detector, we need to have access to its time-dependent dynamics. These can be measured by means of the detector's waiting-time distribution, describing the statistics of time intervals between transport events [60–66]. Importantly, we are able to show that the waiting times can also provide the geometric phases. We study easily realizable models, where the waiting times are accessible through time resolved measurement of the charge state of the system, and provide some recipes for acquiring the geometric phases. At the end, we study some realistic cases of detector errors and comment on detector backaction effects. We argue that none of them can fundamentally hamper the measurement of the topological features.

Finally, through a simple extension of one of the studied models, we briefly show that braid phase transitions in the detector dynamics may open up unexpected applications for new measurement techniques going beyond the detector resolution. Namely, such transitions occurs likewise, when considering a detector whose resolution is not necessarily restricted by some fundamental limit, but rather due to a deficiency.

This paper is structured as follows. In Sec. II we show how the braid topology emerging in the FCS of classical sequential electron tunneling gives rise to such fractional charges. We also perform a comparison to the FCS in Luttinger liquids. In Sec. III we show the emergence of quantized geometric phases defined along the counting field, which depend on the ratio between the fractional charges and the integer charge quantization. In the same section, we demonstrate the analogy to the fractional Josephson effect, known from topological superconducting junctions. Finally, in Sec. IV we provide strategies to verify our claims in experiment, in particular, how to measure geometric phases along the detector degrees of freedom, and point towards applications of topological transitions in the detector dynamics.

II. TOPOLOGY IN FULL COUNTING STATISTICS AND FRACTIONAL CHARGES

A. Fractional charges versus integer charge quantization

To make our main result appreciable, we first need to establish in more detail what is meant by fractional charges. Obviously, we do not claim that transport via sequential electron tunneling literally splits the electron. However, neither do strong quantum correlations. If we partition *any* electronic system along a chosen sharp interface, then we will measure an integer number of electrons on either side, irrespective of the interactions and the topology present in the system. This fact is reflected in the FCS of transport as follows. The central object of interest is the probability $p(N,\tau)$ of having transported N electrons into a given reservoir, after a measurement time τ. The moment generating function is then defined as the Fourier transform of this probability,

$$m(\chi,\tau) \equiv \sum_N e^{i\chi N} p(N,\tau), \tag{1}$$

where χ is referred to as the counting field. Due to the number N of electrons transported being integer, the fundamental charge quantization is embedded in a *global* property of the moment generating function $m(\chi)$. Namely, m is necessarily 2π-periodic in χ.

The previous statement is, however, in conflict with the predictions of field theories where a noninteger valued charge operator emerges (see, e.g., Ref. [3]). Such theories provide fractional charges up to arbitrary statistical moments and thus break the 2π-periodicity. This leads us to the question, how the notion of fractionally charged quasiparticles can be reconciled with the fundamental integer charge quantization? The answer lies in the *local* properties of the moment generating function, respectively, in the analytic continuation of m, when considering the individual cumulants of transport. For this purpose, one defines the cumulant generating function c as $m(\chi) = e^{c(\chi,\tau)\tau}$. Then, the cumulants are obtained through a local Taylor expansion of c around $\chi = 0$,

$$C_k(\tau) = (-ie)^k \partial_\chi^k c(\chi,\tau)\big|_{\chi\to 0}. \tag{2}$$

For instance, the current expectation value is given as $I = C_1$, or the current noise as $S = C_2$. In the simplest possible case of Poissonian transport, where the emission of individual excitations mediating the current is uncorrelated, the charge e^* of a quasiparticle can be extracted using only the lowest two cumulants. Namely, one finds for the Fano factor

$$F \equiv \frac{S}{e|I|} = \frac{e^*}{e}. \tag{3}$$

This was shown for the fractional quantum Hall effect [7–11,19], and for the uncorrelated emission of Cooper pairs [67]. Recently, the occurence of a universal fractional Fano factor has been predicted also for transport through a charge Kondo device [68].

However, we want to define a notion of fractional charges valid well beyond the Poissonian limit, which can be done as follows. We take Ref. [14] as an inspiration, where the FCS for transport through Luttinger liquid nanowires was derived. In that work, the authors show that within the framework of Luttinger liquid theory, the 2π-periodicity of the moment generating function m is indeed broken (again, due to the presence of a noninteger-valued charge operator). As the authors explain, the origin of this violation is due to discarding modulations of the charge density on the length scale of the Fermi wave length—a standard procedure to arrive at Luttinger liquid theory [69]. If, therefore, the transport statistics are measured across a sharp interface (sharp with respect to the Fermi wavelength), then this literal fractionalization of charge cannot be physical. The authors assert that in this case, the moment generating function with broken periodicity is only correct for χ in between $-\pi$ and π, and beyond this interval, m has to be continued periodically—thus reinstating charge quantization at the expense of discontinuities in $m(\chi)$. Importantly, we observe that the fractional charge of the Luttinger quasiparticles remains nonetheless well-defined, as the analytic continuation of the moment generating function beyond the $-\pi$ to π interval. We will comment more on the findings of Ref. [14] later, in Sec. II C. At this stage, we can, however, already summarize the following. The result of Ref. [14] suggests that the picture of fractionally charged quasiparticles is perfectly valid locally in χ, that is, when expanding the moment generating functions into the low cumulants, whereas

care has to be taken with respect to the *global* properties of the moment generating function (i.e., when including cumulants of all orders). In fact, this nontrivial relation between local and global properties of observables along a certain base space (here the counting field χ) already indicates that topological considerations may become important.

In following sections, we will consider topological transitions in the FCS of ordinary sequential electron tunneling, lacking any kind of strong quantum correlations. As we will show, in particular, for long measurement times τ, we will find the exact same feature of a fractional charge extractable from the analytic continuation of the moment generating function m, and a globally conserved 2π-periodicity including discontinuities at $\chi = \pm\pi$. We note that in the context of master equations, a nonanalytic behavior of the moment generating function due to dynamical phase transitions has already been considered [16,70,71]. Here we provide the crucial new insight, that these discontinuities indicate the presence of fractional charges, being at odds with integer charge quantization.

Let us also foreshadow right away, that after that, in Sec. II D, we will strongly generalize this finding to finite measurement times τ. As we hinted at in the introduction, we will show that the system-detector time evolution, described through a set of eigenmodes as a function of χ, see Fig. 1, can be mapped to an auxiliary system with fractionally charged quasiparticles, supplemented with a detector resolving only integer charges. As we will explain in more detail later, the addition of a detector resolving only integer charges e is very similar, and for long τ in fact identical, to the "by hand" reintroduction of charge quantization proposed by Ref. [14]. Unfortunately, however, a complete comparison of the two kinds of quasiparticles for finite τ is currently out of reach: The argument to reinstate integer charge quantization in Ref. [14], in spite of being very plausible, appears without formal derivation. While generalizations of Luttinger liquid theory have been worked out [72], we are not aware of an extension that preserves integer charge quantization [73]. A closer comparison of the here considered effect to strongly correlated systems will, however, be possible for the special case of the fractional Josephson effect in superconducting junctions, as we explain in more detail in Sec. III.

B. Transport statistics of sequential tunneling and braid group

Now, let us fully focus on sequential electron tunneling through small quantum systems, such as quantum dots or metallic islands. We first provide the main assumptions concerning the dynamics of the open quantum system in the absence of transport measurements. Namely, we assume a local system weakly tunnel coupled to two (or more) reservoirs. With weak coupling, we here mean that the timescale at which the electrons tunnel is slower than the timescale $\tau_{\rm res}$ at which correlations in the reservoirs decay. Given the tunneling rate Γ (for a definition see Secs. II C and Sec. S1.1 in the Supplemental Material [74]), the weak coupling picture is valid as long as $\Gamma \ll \tau_{\rm res}^{-1}$. The inverse of $\tau_{\rm res}$ scales with the dominant energy scale given by the reservoir. Close to resonance $\tau_{\rm res}^{-1}$ typically scales with the reservoir temperature. When the chemical potentials of the reservoirs are strongly detuned from the systems energy states, then $\tau_{\rm res}^{-1}$ scales with the difference between said energies and the chemical potential.

Through tracing out the reservoir degrees of freedom, the state of the local system is described by a reduced density matrix. We focus on the simplest possible case, when the dynamics of the system is completely incoherent, such that the reduced density matrix stays diagonal in a given basis (in our case, the charge and energy eigenbasis of the quantum system). In this case, we may discard the offdiagonal elements, and capture the diagonal part of the density matrix as a vector of probabilities, $|P)$. In the weak coupling regime, the time evolution of $|P)$ is given by a fully Markovian master equation,

$$\partial_t |P(t)) = W|P(t)), \tag{4}$$

where W can be represented as a trace preserving matrix, with a set of eigenvalues $\{\lambda_n\}$. It can be decomposed into a sum of contributions, $W = \sum_\alpha W_\alpha$, where each W_α describes the coupling to one reservoir α. We focus on matrices W with a unique stationary state, with eigenvalue $\lambda_0 = 0$, while the other (generally nondegenerate) eigenvalues $\lambda_{n\neq 0}$ have a real part <0. We refer to the corresponding eigenmodes with $n \neq 0$ as decaying modes. We furthermore focus on matrices W, which have, in addition, corresponding left and right eigenvectors, $|n)$ and $(n|$, where the notation is such that any $|a)$ is a vector, whereas any $(b|$ should be regarded as a map $(b|\cdot$ from a vector to a scalar. The right eigenvector to $\lambda_0 = 0$, $|0)$, corresponds to the density matrix of the stationary state, $|0) = \lim_{t\to\infty} |P(t))$. The corresponding left eigenvector $(0|$ is simply the operator tracing over the degrees of freedom of the quantum system, $(0|\cdot = {\rm tr}_S[\cdot]$. Thus, $(0|$ having eigenvalue 0 expresses the trace preserving property of W, i.e., $(0|W = 0$. The decaying modes $n \neq 0$ may likewise have a specific physical interpretation, depending on the system under consideration. For quantum dot systems (as we consider them later) such higher modes correspond to the decay of the charge or spin of the quantum system [75], or even a quantity related to fermion parity [76–79].

Now we come to the measurement of transport. For for the sake of simplicity, but without loss of generality, we limit our considerations to two reservoirs, one left and one right, such that we may write $W = W_{\rm L} + W_{\rm R}$. We now want to relate the system dynamics, Eq. (4) to the probability $p(N, \tau)$, respectively, to the moment generating function m, as defined in Eq. (1).

For this purpose, we describe the FCS by the addition of an explicit detector with a degree of freedom N, coupled to the system such that $N \to N \pm 1$ when an electron exchange is measured. The detector is thus part of the total physical system storing the information of the transport processes [80], and the dynamics of system plus detector can be described in terms of an all-encompassing Hamiltonian operator [30,31,81]. Evaluating $m(\tau)$ consequently corresponds to a projective measurement of the detector state at time τ. Taking into account the composite detector and system degrees of freedom, we receive $|P(t)) \to |P(N, t))$ and $W \to W(N - N')$. The off-diagonal elements in W correspond to all processes where a nonzero charge transport is registered, $N - N' \neq 0$. The resulting

dynamics of system *and* detector is now given as $\partial_t|P(N,t)) = \sum_{N'} W(N-N')|P(N,t))$. We perform again the same Fourier transform, resulting in the equation

$$\partial_t|P(\chi,t)) = W(\chi)|P(\chi,t)). \tag{5}$$

By means of this Fourier transform, it is easy to understand the relation between $W(\chi)$ (for the system-detector dynamics) and $W = W(0)$ (for the system dynamics only). Namely, $\chi = 0$ corresponds simply to tracing over the detector degrees of freedom N, thus discarding the information stored in the detector state, and recovering the system dynamics without the detector.

Equation (5) establishes the combined system-detector dynamics. Note that these dynamics are valid when considering timescales τ slower than the reservoir correlation time, $\tau_{\rm res}$. We refer to this as the low-frequency limit of FCS. Note, however, that due to weak coupling, $\Gamma \ll \tau_{\rm res}^{-1}$, we can not only correctly describe the zero-frequency limit of FCS $\tau^{-1} \ll \Gamma$ (which we also refer to as the long measurement time limit) but also a finite frequency regime, where τ^{-1} is not limited with respect to Γ (as long as Γ, $\tau^{-1} \ll \tau_{\rm res}^{-1}$). Based on these dynamics, we are able compute the moment generating function after a measurement time τ [see Eq. (1)] as

$$m(\chi,\tau) = (0(0)|e^{W(\chi)\tau}|0(0)) \tag{6}$$

$$= \sum_n \alpha_n(\chi) e^{\lambda_n(\chi)\tau}, \tag{7}$$

where we expressed the right-hand side explicitly in terms of the eigenspectrum of $W(\chi)$. That is, $\alpha_n(\chi) = (0(0)|n(\chi))(n(\chi)|0(0))$, where $\lambda_n(\chi)$ and $|n(\chi))$ as well as $(n(\chi)|$ are the eigenvalues, and right as well as left eigenvectors of $W(\chi)$. The labels of all n at finite χ are chosen such that they correspond the same labels for $\chi = 0$. Consequently, with the eigenvalue $\lambda_0(\chi)$ we denote the mode that corresponds to the stationary state for $\chi = 0$, such that $\lambda_0(0) = 0$. In Eq. (7) we assumed the system to be in the stationary state $|0(0))$ initially, which is, however, not a necessary condition for our following results. We note furthermore that we here consider systems where W can be always decomposed into left and right eigenvectors for real χ. In Sec. S2 in the Supplemental Material [74], we do, however, show that there are special, isolated points (commonly referred to as exceptional points) in the space of complex χ, where a decomposition into eigenvectors is not possible. In fact, these points generate the here considered topology (see later in this section, as well as Sec. S2 in the Supplemental Material [74]).

Up until now, we have considered the detector as an actual physical entity, with a measurable state. We want to point out, that there is a different way of formulating and interpreting the FCS, in terms of the current operator $\widehat{I}$ as the observable, i.e., when accessing the transport statistics through explicit current measurements. The expectation value of $\widehat{I}$ and higher cumulants (current noise S, skewness, and so forth) can be related to the moment generating function as we already introduced in Eq. (2). We emphasize the existence of the two notions of FCS, because as we will see in a moment, there are some subtle differences between them in the topological phase. Moreover, note that in the limit of very long measurement times $\tau \to \infty$, one can easily see in Eq. (6), that only the eigenvalue with the lowest real part survives. Thus, for the cumulant generating function, at least locally at χ close to zero, one finds [82,83]

$$c_\infty(\chi) \equiv \lim_{\tau\to\infty} c(\chi,\tau) = \lambda_0(\chi). \tag{8}$$

This limit can be considered as a thermodynamic limit of a macroscopic number of transported electrons.

Importantly, returning now to the picture of an explicit detector, we have so far only specified that we measure the transport into a given reservoir. But we have not yet specified which of the reservoirs. Due to current conservation this does not appear like an important distinction, as the stationary current entering from the left reservoir must be the same as the entering the right reservoir. In fact, not only should it be irrelevant at which reservoir we measure, we should even be able to consider an arbitrary weighted sum of transport measurement at both reservoirs, as long as their sum still provides the same current. There is, however, a subtle issue when considering the topological properties of FCS, and in particular, when discussing geometric phases (see Sec. III), which render such a detailed specification of the measurement scheme necessary.

To appreciate the importance of the measurement setup, let us show that to ensure integer charge quantization, it will be necessary to choose a sharp interface, across which transport is measured (in fact, not unlike the case of FCS in Luttinger liquids [14]). For the here considered small quantum systems (such as quantum dots), this leaves us with two possibilities. Either we place the detector at the interface between the quantum system and the right, or the left contact. For a detector attached to the right (which will be the default setting for the rest of the paper, unless specified differently), the kernel including counting fields can be represented in a compact way as

$$W(\chi) = W_{\rm L} + e^{-i\chi\widehat{n}} W_{\rm R} e^{i\chi\widehat{n}}, \tag{9}$$

where $\widehat{n}$ is a superoperator, defined such that $(0|\widehat{n}|P)$ returns the charge expectation value of the quantum system. We will define $\widehat{n}$ explicitly later, when dealing with explicit models. If we were to measure at the interface to the left reservoir, however, then we would find a different kernel, which can be obtained from the above through the unitary transformation, $e^{i\chi\widehat{n}} W(\chi) e^{-i\chi\widehat{n}}$. Both of these kernels are manifestly 2π-periodic, since $\widehat{n}$ has integer eigenvalues, thus ensuring the 2π-periodicity of $m(\chi)$ [see Eq. (6)], and preserving integer charge quantization. To emphasize the relation between charge quantization and sharp interfaces, let us now consider an example, where the detector is, in some sense, blurry. Imagine a detector that measures currents out of the left and into the right contact, and superposes them with a probability of p and $1-p$, respectively. Such setups are likewise described through a unitary transformation, $e^{i\chi\widehat{n}p} W(\chi) e^{-i\chi\widehat{n}p}$. Because they are related to a unitary transformation, all these kernels will provide the same eigenvalues as the kernel in Eq. (9), and consequently the same cumulants in the long-time limit (due to the aforementioned current conservation). However, while the eigenvalues do not depend on p, the *eigenvectors* do. And the eigenvectors enter in the moment generating function for finite measurement times τ, and, as we see in Sec. III, in the

geometric phases. Thus the unprecise detection schemes, $p \neq 0, 1$, have measurable consequences. In particular, the kernels have a broken 2π periodicity, and thus violate integer charge quantization. In this case, this is, however, not unphysical (similar to the argument in Ref. [14]), because we do not measure across a single sharp interface, but at two interfaces, with a statistical uncertainty $\sim p(1-p)$.

Now, we discuss the topology of the eigenspectrum of $W(\chi)$, as first studied by Ren and Sinitsyn [16]. This notion of topology arises from two ingredients. The first ingredient is the 2π-periodicity of $W(\chi)$ in χ due to the discreteness of the transport process (when measured across a sharp interface), from which follows that at a certain value of χ, $W(\chi)$ has the same set of eigenvalues as at $\chi + 2\pi$. The second ingredient is the continuity of the eigenspectrum as a function of χ, in the sense that locally (in χ) we can always find a labeling n of eigenvalues, such that $\partial_\chi \lambda_n(\chi)$ does not diverge. This allows us to examine, how the eigenvalues are connected in a 2π interval in χ. And as shown in Ref. [16] this connection can be nontrivial, such that the eigenspectrum of the kernel $W(\chi)$ can undergo topological transitions, which are characterized according to the braid group [84].

In fact, as we foreshadowed above, we are able to relate the topology of the eigenspectrum along $\chi \in \mathbb{R}$ to exceptional points in the space of a complex counting field $\chi \in \mathbb{C}$, i.e., isolated points, where certain eigenvalues are degenerate and the corresponding eigenvectors are ill-defined (for more details, see Sec. S2 in the Supplemental Material [74]). To each of the exceptional points, we can assign a generator of the braid group. Thus, depending on the configuration of the exceptional points in the space of the complex counting field, the topology of the eigenspectrum for real χ is described by a certain element of the braid group. This provides us in some sense with a bulk-boundary correspondence. In the 2D space of complex counting fields there emerge special points (exceptional points) which carry a braid generator (similar to a topological charge), which then in turn define the topology of the eigenspectrum along the 1D space of the real counting field. Transitions between different topologies occur through a passing of an exceptional point across the real axis of χ. This provides us furthermore with a concrete argument for the topological protection of the effect. Namely, small variations in the kernel $W(\chi)$ give rise to only small shifts of the exceptional points. Thus, the topology of the eigenspectrum is stable within a connected parameter subspace. Moreover, as we show in Sec. S2 in the Supplemental Material [74], for generic kernels W there is no fundamental symmetry (apart from equilibrium transport, see also later) which forbids the presence of exceptional points, and thus a braid phase transition is always possible, in a generic nonequilibrium setup. The exceptional points will again be important when discussing geometric phases in Sec. III.

Of particular interest in this work is the subgroup of braids whereby the 2π-periodicity of the kernel $W(\chi)$ can be broken on the level of the underlying eigenspectrum. Namely, different eigenvalues can wind around each other when continuously advancing χ by 2π, such that $\lambda_n(\chi + 2\pi) = \lambda_m(\chi)$ with $m \neq n$. We define the periodicity $p_n \in \mathbb{N}$ for a particular eigenvalue n to return to its original value, $\lambda_n(\chi + 2\pi p_n) = \lambda_n(\chi)$. Importantly, from the 2π-periodicity of $W(\chi)$, it follows that the eigenvectors satisfy the same relations as the eigenvalues, in particular, $|n(\chi + 2\pi))(n(\chi + 2\pi)| = |m(\chi))(m(\chi)|$ and $|n(\chi + 2\pi p_n))(n(\chi + 2\pi p_n)| = |n(\chi))(n(\chi)|$. We provide a generic example of a system with five eigenvalues in Fig. 1(a). In this example, we chose a spectrum which is composed of two braid subblocks that have a different periodicity. In the example of Fig. 1, $\lambda_0(\chi + 2\pi) = \lambda_1(\chi)$ and $\lambda_1(\chi + 2\pi) = \lambda_0(\chi)$, as well as $\lambda_2(\chi + 2\pi) = \lambda_3(\chi)$, $\lambda_3(\chi + 2\pi) = \lambda_4(\chi)$, and $\lambda_4(\chi + 2\pi) = \lambda_2(\chi)$.

Finally, let us stress that, due to the overall 2π-periodicity of $W(\chi)$, the breaking of the periodicity on the level of the eigenvalues and eigenvectors goes hand in hand with a *redundancy*. That is, the individual eigenvalues and eigenvectors in the same braid subblock are merely shifted images of each other, and thus contain all the same information. This fact will be of importance in Sec. II D. Considering the eigenvalues as a function of χ as generalized, complex bands, and χ as a detector momentum [85], we may regard the braid phase transition with a breaking of periodicity as a merging of bands. We account for the resulting redundancy by assigning a new band index ν, which does not count individual eigenvalues, but enumerates individual (braided) subblocks (i.e., the actual independent bands). This is illustrated in Fig. 1(b), where the spectrum has been projected onto the complex plane. Here, the eigenvalues $n = 0, 1$ form the new topological band $\nu = 0$, and the eigenvalues $n = 2, 3, 4$ form the band $\nu = 1$. In essence, enumerating the eigenvalues with the index n is meaningful when looking at the spectrum locally (at a specific value of χ), whereas the index ν is meaningful for indexing the eigenspectrum globally, i.e., when putting it into relation with the global 2π-periodicity of W.

In the following, we will argue that the periodicity breaking due to the nontrivial topology results in a transport statistics in terms of *fractional* charges in the same sense as it occurs in the above-mentioned strongly correlated systems. Each of the bands ν provides a separate fractional charge $e^*_\nu = e/p_\nu$. That is, in the example given in Fig. 1, the band $\nu = 0$ has a fractional charge of $e/2$, and the band $\nu = 1$ contributes to the transport with a charge $e/3$. In the next sections, we will provide a careful argumentation for the fractional effect, and show that it is, as a matter of fact, an extremely common occurrence in many simple transport situations.

C. Fractional charges of the stationary state

We first want to establish the emergence of a fractional charge in quantum dot systems for the stationary mode $n = 0$, i.e., when focusing on a transport measurement in the limit of long measurement times $\tau \to \infty$. For this purpose, we discuss the simplest generic transport model, the single-level quantum dot, where a braid phase transition occurs for the stationary state for a sufficiently strong out-of-equilibrium bias, leading to a fractional charge $e/2$. We then extend the model to a serial double quantum dot, where, in addition, a fractional charge $e/3$ can occur in the stationary state. For the latter model, we also discover topological phases with a trivial stationary state, but nontrivial decaying modes, requiring an understanding of fractional charges beyond the long measurement time limit.

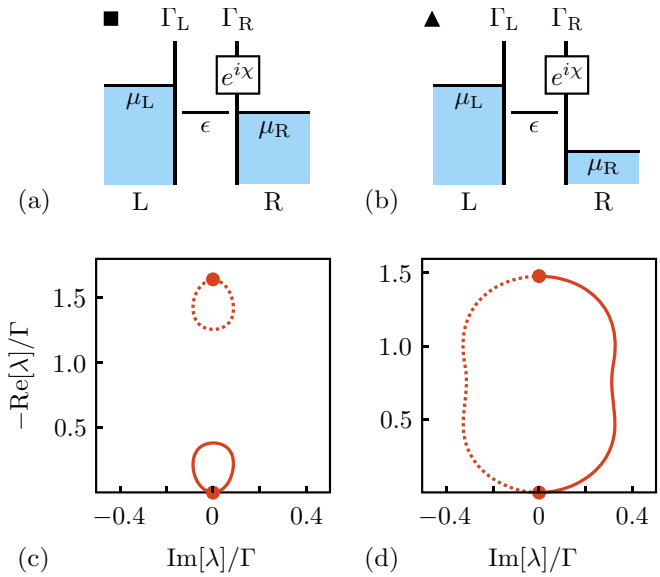

FIG. 2. (a) Single-level quantum dot system, where the transport statistics are measured between dot and right reservoir. The bias and energy configuration correspond to the point marked with a square in Fig. 3(a), where the transport is trivial. (b) The same quantum dot system, however, in a different configuration, marked by a triangle in Fig. 3(a), where the transport is in the topological phase. (c), (d) Projection of the complex eigenspectrum of $W(\chi)$, see Eq. (12), for the same parameters as in Fig. 3(a), at the square point $\mu_L - \epsilon = k_B T$ and $\mu_R - \epsilon = 0$ (c) and at the triangle point $\mu_L - \epsilon = k_B T$ and $\mu_R - \epsilon = -2k_B T$ (d). In (d) the spectrum is braided in such a way, that the two eigenvalues have a 4π-periodicy, corresponding to a charge $e/2$. The solid points indicate the eigenvalues for $\chi = 0$.

1. Single-level quantum dot

Let us begin with the simplest possible model of a single-level quantum dot coupled to two reservoirs. As we will argue now, there occurs a topological phase where the transport is correctly described in terms of fractional charges. We then put this result in relation with the FCS obtained in Luttinger liquid nanowires [14]. Crucially, even though the two systems are physically very different, we will find that the moment generating function provides the *same* signatures of fractional charges for both systems.

We assume that a single-level quantum dot has very low capacitances, such that the energy associated with charging the system is far greater than the temperature. Let us set the energy of the single quantum dot level such that it is in the resonant configuration, where only a transition between the empty and the singly filled level, $|0\rangle$ and $|1\rangle$, is possible (we take into account the possibility that the state $|1\rangle$ may be spin-degenerate). We weakly couple the dot to two ordinary metallic reservoirs, one left and one right, and we measure the transport statistics at the tunnel contact to the right reservoir; see Figs. 2(a) and 2(b). The full Hamiltonian is described in Sec. S1.1 in the Supplemental Material [74].

The state of the quantum dot can be described by a (diagonal) density matrix, which reads, in vector form, $|P) = (P_0, P_1)^T$, where P_0 and P_1 are the probability to be in either of the two charge states. The corresponding kernel for weak tunnel coupling reads

$$W(\chi) = W_L + e^{i\chi\hat{n}} W_R e^{-i\chi\hat{n}}, \tag{10}$$

with $\hat{n} = \mathrm{diag}[(0, 1)]$ and [86]

$$W_\alpha = \begin{pmatrix} -\sigma\Gamma_\alpha f_\alpha & \Gamma_\alpha[1 - f_\alpha] \\ \sigma\Gamma_\alpha f_\alpha & -\Gamma_\alpha[1 - f_\alpha] \end{pmatrix}, \tag{11}$$

where $\alpha = \mathrm{L,R}$, and σ indicates the degeneracy of the quantum dot level, e.g., for the ordinary spin-degenerate case, $\sigma = 2$. The transition rates are given by the tunnling rates Γ_α and the Fermi functions, $f_\alpha = 1/(1 + e^{\beta[\epsilon - \mu_\alpha]})$, where β is the inverse of the thermal energy $k_B T$, and the energy differences $\epsilon - \mu_\alpha$ are controlled by gate and bias voltages. We furthermore define the sum of tunneling rates $\Gamma = \Gamma_L + \Gamma_R$. Importantly, with the same kernel, we may also describe metallic islands instead of quantum dots on a similar footing [86]. Therefore, while for the remainder of this section we focus on the quantum dot case, we stress that the results discussed below hold qualitatively also for metallic islands.

The spectrum of $W(\chi)$ in Eq. (10) has two eigenvalues, $\lambda_0(\chi)$ and $\lambda_1(\chi)$, which are given as

$$\lambda_{0,1}(\chi) = -\frac{\gamma_c}{2}[1 \mp \sqrt{1 + u(\chi)}], \tag{12}$$

with

$$u(\chi) = r_+(e^{i\chi} - 1) + r_-(e^{-i\chi} - 1), \tag{13}$$

and $\gamma_c = \sum_\alpha (\sigma\Gamma_\alpha f_\alpha + \Gamma_\alpha f_\alpha^-)$ is the charge relaxation rate, such that $\lambda_1(\chi = 0) = -\gamma_c$ (see also Ref. [75]), and $r_+ = 4\sigma\Gamma_L\Gamma_R f_L f_R^-/\gamma_c^2$ as well as $r_- = 4\sigma\Gamma_L\Gamma_R f_L^- f_R/\gamma_c^2$. We find that $0 \leqslant r_\pm \leqslant 1$, with the constraint $0 \leqslant r_+ + r_- \leqslant 1$. Note also that at $\chi = 0$, $u = 0$. Crucially, while Eq. (12) is a well-known result [15,22,87], we here argue that it has not yet been interpreted to its fullest extent.

As a first step, we point out that for these two eigenvalues, we encounter two distinct topological phases, in accordance with [16]. The spectrum is either trivial, as depicted in Fig. 2(c), or topological with a 4π-periodicity, as depicted in Fig. 2(d). In the latter case, the two eigenvalues $\lambda_{0,1}$ merge into one single band $\lambda_{v=0}$. The occurrence of the topological phase can be easily understood in terms of basic complex analysis, when considering $u(\chi)$; see Eq. (13). For $r_+ + r_- < 1/2$, $u(\chi)$ does not enclose the point -1 when drawing it as a complex contour for χ from 0 to 2π. Here, the spectrum is trivial, as we can always evaluate the square root in Eq. (12) for all χ without having to take into account the branch cut. As soon as $r_+ + r_- > 1/2$, $u(\chi)$ does enclose the point -1, and the eigenspectrum is topological, as the branch cut is unavoidable.

Importantly, as we stated already, the topological phase appears within a connected parameter subspace, see Figs. 3(a) and 3(b), and is thus stable with respect to small variations of the system parameters. The configurations that favour the topological phase are for strong bias, where the transport goes predominantly in one direction; see Fig. 2(b). For the special case of zero bias, however, the braid phase transition is not possible (as also pointed out by Ref. [16], see also Sec. S2.2 in the Supplemental Material [74]). Namely, in equilibrium, the eigenspectrum of W is real for all χ (due to symmetries based on microreversibility [88,89]), and is, in general,

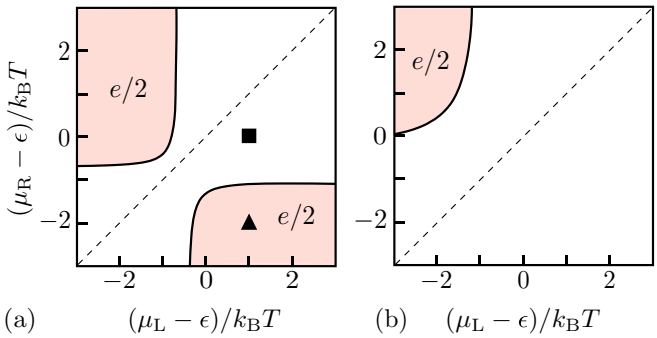

FIG. 3. The different topological phases of transport through the single-level quantum dot, with the corresponding fractional charge for various parameters, as a function of $\mu_L - \epsilon$ and $\mu_R - \epsilon$. Red areas correspond to fractional charge $e_0^* = e/2$. The tunneling asymmetry is different for the two panels, $\Gamma_L/\Gamma = 0.6$ for (a) and $\Gamma_L/\Gamma = 0.8$ (b), respectively.

gapped, with an ordinary 2π-periodicity. As we will discuss later (in Sec. III B), topological Josephson junctions provide an exception, where the transport dynamics is described by an operator with a real spectrum with broken periodicity. This, however, requires extra conditions, which are satisfied thanks to the presence of the nontrivial superconductors (see also S2.3 in the Supplemental Material [74]). Finally, the topological phase in W is inhibited likewise for strongly asymmetric tunnel coupling (even in the presence of a strong bias), because strong coupling asymmetry leads to one of the two tunnelings being the bottle neck process. This results in eigenvalues which are far apart, and do thus not engage in a braid phase transition.

In fact, even though it is hard to predict the topology of the eigenspectrum for a general matrix $W(\chi)$ without explicitly calculating it, the above realizations can serve us to give at least some rudimentary recipes, which are valid beyond the currently considered simple single-level model. To create a system with a nontrivial topology, one should generally avoid being close to equilibrium. As just stated, in equilibrium, the eigenspectrum is real, and is therefore, in general, gapped (again, unless additional symmetries are present, see Sec. III B). Second, processes occurring with strongly different timescales (such as the strongly asymmetric tunnel coupling mentioned above) give rise to strongly separated eigenvalues that do not partake in a braid phase transition. A third point relates to the fact that in the above kernel, we did not include energy levels and charge states, that are either significantly above or below the energy window spanned by the two chemical potentials. These additional states decay in principle with similar rates as the active states $|0, 1\rangle$ (at least if the tunneling rates are only weakly energy-dependent), and thus they do not provide a separation of timescales. However, such levels do not contribute to the transport as they are either always empty, or always filled. This fact manifests on the level of the eigenspectrum as eigenvalues that depend only very weakly on χ. Such eigenvalues do likewise not partake in a braid phase transition.

Let us now look at the moment generating function in the long measurement time limit $\tau \to \infty$. Here, only the eigenvalues with the real part closest to zero survive, see Eq. (7). While for a trivial spectrum this simply means that the moment generating function is given by a single mode, $m(\chi, \infty) = \lim_{\tau\to\infty} e^{\lambda_0(\chi)\tau}$, for the topological spectrum, m becomes discontinuous,

$$m(\chi, \infty) = \lim_{\tau\to\infty} \begin{cases} e^{\lambda_0(\chi)\tau} & \text{for } \mathrm{Re}[\lambda_0(\chi)] > \mathrm{Re}[\lambda_1(\chi)] \\ e^{\lambda_1(\chi)\tau} & \text{for } \mathrm{Re}[\lambda_0(\chi)] < \mathrm{Re}[\lambda_1(\chi)] \end{cases}. \quad (14)$$

As we see, the moment generating function remains 2π-periodic, while the analytic continuation of m around $\chi = 0$ leads to a broken periodicity in χ. However, which of the two will be measured? Crucially, the 2π-periodic result will be automatically found by an experimenter having explicitly access to a detector attached to the right reservoir, as introduced in Sec. II B. Namely, such an experimenter will directly measure $p(N, \tau)$ and consequently, m will be 2π-periodic by construction. Let us contrast this to a different experimenter, who has access to the cumulants $C_k(\tau \to \infty)$, e.g., by measuring the expectation values of the current operator $\hat{I}$ and its higher order correlations for very long times [see Eqs. (2) and (8) in Sec. II B]. The latter experimenter will not observe the discontinuity. Instead, by reconstructing the cumulant generating function through a Taylor series $c(\chi) = \sum_k (i\chi/e)^k C_k/k!$ and performing the analytic continuation, he must come to the conclusion that a physical fractional charge of $e/2$ is present. He simply performs a Fourier analysis back from χ to charge space, and he will thus find that the system should be described by a charge operator with noninteger eigenvalues. This latter nonphysical finding is due a subtle issue concerning the order of limits. Namely, the convergence of the cumulant generating function for finite χ depends on how long one really measures, and to how many orders one sums up the cumulants. The fractional charge would appear to become physical when the limit $\tau \to \infty$ is taken first. This result may to some extent be considered unproblematic, since in this limit the number of charges transported is infinite. However, in reality, of course, no experiment goes on forever, which means that this result has to be interpreted with care. Thus, we can clearly see now the importance of the explicit presence of a detector: it resolves this issue also in the limit $\tau \to \infty$, and reinstates charge quantization for all times τ.

We now relate this result to the example of FCS in strongly correlated transport, which we introduced already in Sec. II A. As we explained there, in Ref. [14], the authors study the transport through a 1D nanowire with an interacting region. In the limit where the measurement time τ is short with respect to the plasmon time-of flight, but long with respect to inverse energy scale given by the quasiparticle distributions, they find for the cumulant generating function,

$$c(\chi) = \sum_{l=0}^{\infty} \int \frac{d\epsilon}{2\pi} \{\ln[1 + (e^{i\chi e_l^*} - 1) n_L(\epsilon)] + \ln[1 + (e^{-i\chi e_l^*} - 1) n_R(\epsilon)]\}, \quad (15)$$

where the transport is a sum of left (L) and right movers (R), with their corresponding occupation number $n_{L,R}$, which are split into quasiparticles with fractional charges $e_l^* \in \mathbb{R}$. Unlike the FCS in a single-level quantum dot, there is an additional sum over energies, since there are no localized levels, and instead a continuum of energy channels is available

in the region between the contacts. Therefore, to make the previous result more relatable to our quantum dot system, let us consider the contribution of just one energy channel, ϵ. In addition, let us assume a small quasiparticle occupation for this particular energy $n_\alpha(\epsilon) \ll 1$, where

$$c_\epsilon(\chi) \approx \sum_{l=0}^{\infty} \{(e^{i\chi e_l^*} - 1)n_{\rm L}(\epsilon) + (e^{-i\chi e_l^*} - 1)n_{\rm R}(\epsilon)\}, \quad (16)$$

that is, we recover a sum of Poissonian transport events with different charges e_l^*. As we will see in a moment, we can find an expression of the same structure for sequential electron transport in a particular limit; see Eq. (17). But first, let us note that the moment generating function $m(\chi) = e^{\tau c(\chi)}$, with c given in Eq. (16), is manifestly not 2π-periodic in χ, violating charge quantization. In Ref. [14], the authors notice this violation, and assert that is a consequence of neglecting charge fluctuations on the length scale of the Fermi wave length (referring to [69]). If transport is measured across a sharp interface, then the moment generating function is, according to Ref. [14], only correct for $-\pi < \chi < \pi$, and then has to be continued periodically. This forced periodicity comes, just like in our example of conventional sequential electron tunneling, at the expense of discontinuities in m at $\chi = \pm\pi$. As we see, when considering the FCS, the fractional charge is again not a property that can be defined for the fully physical m. It can, however, nonetheless be defined through the analytic continuation of the moment generating function m. This is a striking analogy of the transport statistics of two extremely different systems. The only difference concerns the values of the fractional charges. Namely, the charges in Luttinger liquid physics, e_l^*, can, in general, be irrational. The actual expressions for e_l^* depend on the details of the system [14]. We refrain from discussing them in detail, as this is not the focus of our work.

At this point, let us repeat that in Refs. [15,22] the idea of fractional charges in sequential tunneling has already been coined, even though only in a special limit. Namely, they find a cumulant generating function of the form

$$c(\chi) = \gamma(e^{i\chi/2} - 1), \quad (17)$$

and note that this looks like the Poissonian statistics of a $e/2$ particle. We can recover the same result in Eq. (12), when setting the tunneling rates to $\sigma\Gamma_{\rm L} = \Gamma_{\rm R} = \gamma$, and the reservoir occupations to $f_{\rm L} = 1$ and $f_{\rm R} = 0$ (that is, for a very strong bias). In particular, in Ref. [15], the authors advised against taking this fractional charge too seriously, arguing very plausibly that single electron transistors "do not chop electrons in half." However, as we already insisted upon in the introduction and on several occasions in this section, the same is true for strongly correlated systems: electrons can very generally not be split in a literal physical sense, and it is paramount that the moment generating function retain its 2π-periodicity. Second, and very importantly, in Refs. [15,22] the fundamental connection between fractional charges and braid phase transitions has not been considered. The occurrence of fractional charges is *not* some freak coincidence for very special chosen parameters, but is a stable topologically protected property occurring in a large, connected parameter subspace. Moreover, the question is not whether a certain physical effect, be it topological transitions in the FCS, or strong quantum correlations in Luttinger liquids, literally produces fractional charges—neither of them do. The question is, whether the nature of fractional charges occurring in strongly correlated systems *differ* from the ones occurring in conventional sequential electron tunneling, such that they can be differentiated through a transport measurement. We here conclude, that on the level of the transport statistics in a long measurement time regime, we find no qualitative features to tell them apart. In the next section, Sec. II D, we strongly generalize this statement. In fact, we will provide a concrete argument allowing for the interpretation of *all* the eigenmodes of the system-detector dynamics (i.e., not only the stationary mode λ_0) in terms of fractional charges.

2. Quantum dots in series

However, before embarking on a general interpretation of higher modes as fractional charges, let us briefly introduce a system which actually produces nontrivial decaying modes. For this purpose, we consider a quantum dot system with more than a single level. For the previous example, we had only two available states (empty and filled). This naturally limits the number of different topological phases we can observe. For one, we cannot observe a fractional charge of more than $1/2$, due to only having two states. For another, we cannot hope to see a periodicity breaking which does not involve the stationary state. For the more complicated model presented now we will see a much richer topological phase diagram.

We consider two quantum dots in series; see Fig. 4(a). We assume yet again that the individual dots have very high charging energies, and that the gates are tuned such that only the transitions between the three charge states $|00\rangle$, $|10\rangle$, and $|01\rangle$ (i.e., zero extra charges, or a left or right extra charge) are available. As for the charge exchange between the two dots, we focus on a regime where the interdot transport is dominated by an inelastic, incoherent process. For the full Hamiltonian description of this model, consult Sec. S1.2 in the Supplemental Material [74].

We may thus capture the dynamics again by means of a fully diagonal density matrix, with the vector of probabilities $|P) = (P_{00}, P_{10}, P_{01})$, and through the kernel

$$W(\chi) = W_{\rm L} + W_{\rm LR} + e^{i\chi\hat{n}_{\rm R}} W_{\rm R} e^{-i\chi\hat{n}_{\rm R}}, \quad (18)$$

with $\hat{n}_{\rm L} = {\rm diag}[(0,1,0)]$ and $\hat{n}_{\rm R} = {\rm diag}[(0,0,1)]$. The matrices

$$W_{\rm L} = \begin{pmatrix} -\sigma\Gamma_{\rm L} f_{\rm L} & \Gamma_{\rm L}[1-f_{\rm L}] & 0 \\ \sigma\Gamma_{\rm L} f_{\rm L} & -\Gamma_{\rm L}[1-f_{\rm L}] & 0 \\ 0 & 0 & 0 \end{pmatrix}$$

$$W_{\rm R} = \begin{pmatrix} -\sigma\Gamma_{\rm R} f_{\rm R} & 0 & \Gamma_{\rm R}[1-f_{\rm R}] \\ 0 & 0 & 0 \\ \sigma\Gamma_{\rm R} f_{\rm R} & 0 & -\Gamma_{\rm R}[1-f_{\rm R}] \end{pmatrix},$$

account for the sequential tunneling to and from the contacts, where the Fermi functions are now $f_{\rm L,R} =$

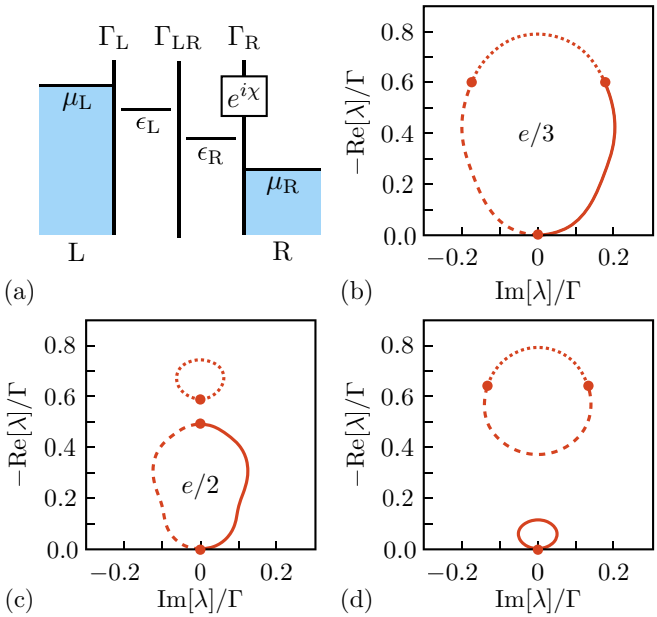

FIG. 4. (a) The model with two quantum dots in series, with the energies $\epsilon_{L,R}$, and the sequential electron tunneling rates $\Gamma_{L,LR,R}$. The transport statistics are measured at the interface between the right dot and the right reservoir. In (b)–(d) we show the three distinct topological phases that occur in the system-detector dynamics. In (b) all three eigenvalues merge into one band with fractional charge $e^* = e/3$. Alternatively, the lowest two eigenvalues can merge into a band with charge $e^* = e/2$, see (c). Finally, the upper two eigenvalues can merge into one band. The parameters for (b)–(d) are $\Gamma_L = \Gamma_R = 0.3\Gamma$ and $\Gamma_{LR} = 0.4\Gamma$, with $\Gamma = \Gamma_L + \Gamma_R + \Gamma_{LR}$ as well as $\mu_L = 2k_BT$, $\mu_R = -2k_BT$ and $\epsilon_R = k_BT$. The remaining parameter is $\epsilon_L/k_BT = \{0, 1.5, 3.2\}$ for (c), (b), and (d), respectively.

$1/(1 + e^{\beta[\epsilon_{L,R} - \mu_{L,R}]})$. The matrix

$$W_{LR} = \begin{pmatrix} 0 & 0 & 0 \\ 0 & -\gamma_{R\to L} & \gamma_{L\to R} \\ 0 & \gamma_{R\to L} & -\gamma_{L\to R} \end{pmatrix}, \tag{19}$$

accounts for the tunneling between the two dots. The specific shape of $\gamma_{L\to R}$, $\gamma_{R\to L}$ will depend on the details of the mechanism mediating the interdot tunneling process, e.g., through electron-phonon mediated tunneling [90,91]. For the sake of simplicity, we assume that they are of the form $\gamma_{L\to R} = \Gamma_{LR} f(\epsilon_L - \epsilon_R)$, $\gamma_{L\to R} = \Gamma_{LR} f(\epsilon_R - \epsilon_L)$, resulting in temperature dependent rates, where for large detuning, $|\epsilon_L - \epsilon_R| \gg k_BT$, there remains simply a constant rate towards the lower lying level (neglecting any energy-dependence of Γ_{LR}). For one, we stress that since we are merely interested in studying the general topological properties, it is not necessary to take into account more details. Second, we point out that the same simple energy dependence for the inelastic rate was successfully used to describe inelastic tunneling in a two-atom electron pump [92].

As for the topology of the transport, we numerically determine the eigenvalues of W in Eq. (18), and thus find the following. Apart from the trivial phase with three independent bands, the system with two quantum dots (islands) in series gives rise to three distinct topologically nontrivial phases. They are depicted in Figs. 4(b)–4(d). In Fig. 4(b) all three eigenvalues form a single band, while in Fig. 4(c), the two lower eigenvalues form the same topological stationary mode as in the previously discussed single quantum dot. We can also observe a topological phase, where the stationary mode is trivial, while the two decaying modes are braided, see Fig. 4(d).

In close analogy to the previous discussion, the first two topological phases [Figs. 4(b) and 4(c)], again give rise to fractional charges in the stationary mode. In particular, for the first topological phase [Fig. 4(b)], there may occur a charge $e/3$.

The third topological phase [Fig. 4(d)] will, however, provide trivial statistics in the here considered limit of long measuring times. In the following section, we will analyze the interplay between system and transport detector from a very different vantage point, and for finite τ. This allows for a much more general interpretation of the topological phases as fractional charges, including the decaying modes, as in Fig. 4(d).

D. Braid phase transition and detector resolution

As we have seen, charge quantization is important to correctly describe the global properties of the moment generating function, and that fractional charges can be well-defined in the infinite measurement time limit as the analytic continuation of m in χ. Now, we want to generalize our findings to finite measurement times, and moreover to general transport situations beyond the sequential tunneling approximation.

To do so, we propose an analogy between charge quantization and the notion of a detector with a minimal resolution limit. To begin, let us consider a very general, out-of-equilibrium transport model with two reservoirs, exchanging particles with a given charge through some tunneling contact. As just announced, we here consider a very generic transport situation, and rely no longer on a weak tunneling approximation. Moreover, we now explicitly deviate from the charge quantization requirement, such that the eigenvalues of the charge operators in the reservoirs do not necessarily need to be a multiple integer of e. Let us first restrict our discussion to the case, where only a single type of charge is exchanged, called e^*. We supplement such a general system with an idealized charge detector, measuring the transport into one of the reservoirs, with the following two properties. First, it has a continuous degree of freedom, here denoted as $\mathcal{E}$, corresponding to an infinitely precise charge resolution. Second, it is ideally coupled to the system, such that whenever there is a transport event passing a certain charge e^* into or out of the reservoir, the detector state receives a kick, such that $\mathcal{E} \to \mathcal{E} \pm e^*$. We may describe the corresponding detector state with a density matrix $\rho(\mathcal{E}, \mathcal{E}')$, providing the probability density $P(\mathcal{E}) \equiv \rho(\mathcal{E}, \mathcal{E})$. Let us assume that at the initial time $t = 0$ the detector state is reset, $\mathcal{E} = 0$. Then, the probability density at the measurement time $t = \tau$ (where the detector state is projected onto the charge eigenbasis) must be of the form [see also Fig. 5(a)]

$$P(\mathcal{E}, \tau) = \sum_N P(N, \tau)\delta(\mathcal{E} - e^*N). \tag{20}$$

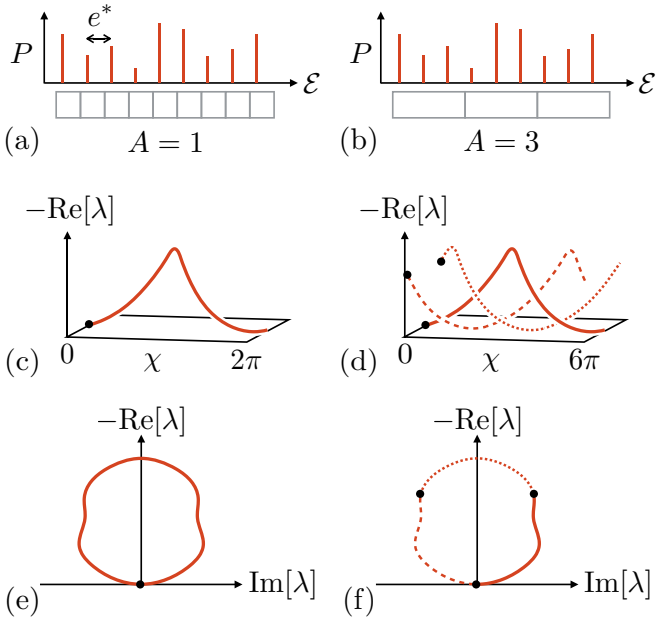

FIG. 5. The concept of detectors with insufficient resolution. In (a) we show the probability density p as a function of $\mathcal{E}$ for an ideal detector, measuring the transport statistics of a particle with charge e^*. Below the $\mathcal{E}$-axis, we indicate a discretized (pixelated) detector with limited resolution e. Here, we suppose that $e = e^*$ ($A = 1$). In (b) a discretized detector with resolution $A = 3$ is shown, that is $e = 3e^*$. The charge transport can no longer be resolved exactly. (c) A generic depiction of a complex eigenmode λ as a function of χ, appearing in the detector dynamics. (d) The eigenmodes $\widetilde{\lambda}_a$ as a function of χ appearing in the time evolution of the detector state with insufficient resolution, $A = 3$. We see that the insufficient resolution results in the appearance of shifted copies of $\lambda(\chi)$, resulting in the same type of braid topology as in Fig. 1. (e), (f) The spectra of (c) and (d), respectively, are projected onto the complex plane, for $0 \leqslant \chi < 2\pi$. The black dots indicate the eigenvalues at $\chi = 0$.

Through a Fourier transform, we receive $P(\chi,\tau) = \int d\mathcal{E} e^{i\frac{\chi}{e}\mathcal{E}} P(\mathcal{E},\tau) = \sum_N e^{i\frac{e^*}{e}\chi N} P(N,\tau)$. We see now that the discreteness of charge e^* corresponds to a periodicity of $P(\chi,\tau)$ in χ, here, however, with period $2\pi e/e^*$.

Now we render the detector nonideal, by introducing a finite resolution in form of "pixels," which may have a size different from e^*. In fact, we set the pixel to the elementary charge e. Based on the entire previous discussion, this pixelation can be motivated by multiple different reasons. As far as the FCS of sequential tunneling are concerned, we note that in the models we considered so far, the detector is locally attached to the interface of one reservoir (the right one, in the above examples), and is by construction "blind" to all charge transfer processes that do not change the charge in said reservoir. These include, for instance, the tunneling into the quantum system from the left reservoir, or the tunneling processes within the quantum system (e.g., the interdot tunneling in the double quantum dot). In a very similar way, we can think of the pixelated detector as "blind," since it does not register any events that occur within the same pixel.

We can, however, motivate the pixelation also in a similar spirit to the FCS of Luttinger liquids presented in Ref. [14]. Namely, a detector with pixel size e can be understood as an *ad hoc* recipe to reintroduce integer charge quantization to a theory that breaks it. This treatment is in fact very similar to the "by hand" reintroduction of charge quantization that the authors of Ref. [14] propose themselves. We will comment in more detail on the similarities and differences to Ref. [14] below.

Finally, a third motivation for the detector pixelation will be exploited in Sec. IV D, where we consider a possible application of topological detector dynamics when the detector has a limited resolution rather due to a deficiency than due to a fundamental limit.

To proceed, we define the nonideal detector probability as $\widetilde{P}(M) = \int_{\mathcal{E}_0+\mathcal{A}M}^{\mathcal{E}_0+\mathcal{A}M+\mathcal{A}} d\mathcal{E} P(\mathcal{E})$, such that all measurement outcomes in the interval $\mathcal{E}_0 + \mathcal{A}M \leqslant \mathcal{E} \leqslant \mathcal{E}_0 + \mathcal{A}M + \mathcal{A}$ get projected onto a discrete detector state $M \in \mathbb{Z}$, where $\mathcal{A}$ is the resolution of the nonideal detector, and $\mathcal{E}_0$ is an arbitrary and irrelevant shift (for simplicity, we require $0 < \mathcal{E}_0 < \mathcal{A}$). For our purposes, it is sufficient to consider a resolution $\mathcal{A}$ which is an integer multiple of e^*, $\mathcal{A} = Ae^*$, $A \in \mathbb{N}$ [see Figs. 5(a) and 5(b)]. Then, we find that the probability distribution of the discretized detector is

$$\widetilde{P}(M,\tau) = \sum_{a=0}^{A-1} P(AM + a, \tau). \tag{21}$$

Thus, the projected state M sums up the probabilites of being in the states N that are within an interval from $N = AM$ to $N = AM + A - 1$. We then likewise perform a Fourier transform for the projected state M, $\widetilde{P}(\chi,\tau) = \sum_M e^{iM\chi}\widetilde{P}(M,\tau)$. We note that for $A = 1$, $\widetilde{P}(\chi,\tau) = P(\chi,\tau)$, which means that if the resolution of the discrete detector matches e^*, we have not actually changed the detector dynamics, as can be expected.

Now we consider the nonideal case, $A > 1$. For the sake of simplicity, let us assume that the dynamics of the original detector state can be described through a single mode, $P(\chi,\tau) = \alpha(\chi)e^{\lambda(\chi)\tau}$ [for a generic example, see Figs. 5(c) and 5(e)]. We note that while the description of the detector dynamics in terms of such eigenmodes is obviously motivated by our considerations of sequential tunneling, it is by no means restricted to this regime, see, e.g., the result of Ref. [14], and references therein. Requiring that $\lambda(\chi)$ and $\alpha(\chi)$ both be analytic, one can show in a straightforward manner that for the nonideal detector

$$\widetilde{P}(\chi,\tau) = \sum_{a=0}^{A-1} \widetilde{\alpha}_a(\chi) e^{\widetilde{\lambda}_a(\chi)\tau}, \tag{22}$$

with

$$\widetilde{\lambda}_a(\chi) = \lambda\left(\frac{\chi + 2\pi a}{A}\right) \tag{23}$$

and

$$\widetilde{\alpha}_a(\chi) = \frac{1}{A}\sum_{a'=0}^{A-1} e^{-i\left[\frac{\chi+2\pi a}{A}\right]a'} \alpha\left(\frac{\chi + 2\pi a}{A}\right). \tag{24}$$

The previous result is obtained by using the periodic δ function,

$$\sum_M e^{iM(\chi - A\chi')} = \frac{2\pi}{A} \sum_m \delta\left(\chi' - \frac{\chi + 2\pi m}{A}\right). \tag{25}$$

We see that the time evolution for the discretized detector with insufficient resolution gives rise to a superposition of modes $\widetilde{\lambda}_a(\chi)$, which are simply shifted copies of the original $\lambda(\chi)$, stretched to a new periodicity $2\pi A$, and braided [see Figs. 5(d) and 5(f)]. And the same is true for the coefficients $\widetilde{\alpha}_a(\chi)$. Thus, the new moment generating function provides eigenmodes with the exact same properties—broken periodicity and redundancy—as the topological subbands introduced in Sec. II B.

Crucially, if we now return to the model systems with sequential electron tunneling, Sec. II C, we find that the detector statistics exhibit a topological eigenspectrum with broken periodicity, even though the detector is ideal in the sense that it measures exactly the electrons that physically tunnel into a reservoir. The braid phase transition does not come from a coarse-grained measurement, but stems from the extra degrees of freedom of the quantum system to which the detector is insensitive. Here, we study rather generically the dynamics of a detector with a finite resolution that does not necessarily match the unit of a certain discrete process - and we make the striking observation, that also here the same topological eigenspectrum with broken periodicity occurs: the broken periodicity directly relates to the mismatch between the detector resolution (e) and the subpixel size of a discrete process (e^*). Therefore, we conclude that if the dynamics of the detector state is the only accessible information, then the nontrivial transport statistics with periodicity p of regular electrons are *topologically indistinguishable* from trivial transport of fractional charges e/p, measured with a detector with resolution e.

Importantly, we can easily generalize the previous procedure to the case where the detector dynamics $P(\chi, \tau)$ contains more than just a single mode. Consequently, the equivalence between braid phase transitions and finite detector resolution can be easily extended to the decaying modes. For this purpose, we start with the cumulant generating function as given in Eq. (7). Taking then into account the redundancy due to broken periodicity, we can reexpress the moment generating function in terms of the reduced band index ν, such that

$$\begin{aligned} m(\chi, \tau) &= \sum_n \alpha_n(\chi) e^{\lambda_n(\chi)\tau} \\ &= \sum_\nu \sum_{a=0}^{p_\nu} \widetilde{\alpha}_{\nu,a}(\chi) e^{\widetilde{\lambda}_{\nu,a}(\chi)\tau}, \end{aligned} \tag{26}$$

where $\widetilde{\lambda}_{\nu=0,0}(\chi) = \lambda_{n=0}(\chi)$ and $\widetilde{\lambda}_{\nu=0,1}(\chi) = \lambda_{n=1}(\chi)$ as well as $\widetilde{\lambda}_{\nu=1,0}(\chi) = \lambda_{n=2}(\chi)$, $\widetilde{\lambda}_{\nu=1,1}(\chi) = \lambda_{n=3}(\chi)$, and $\widetilde{\lambda}_{\nu=1,2}(\chi) = \lambda_{n=3}(\chi)$, and similarly for the coefficients α. From this equation, we can find a corresponding auxiliary system describing a transport with explicit fractional charges, and a detector with the resolution limit of e, giving rise to the exact same moment generating function.

We thus conclude, that the detector dynamics in Fig. 1 is equivalent to the coexisting transport of $e/2$ and $e/3$ charges,

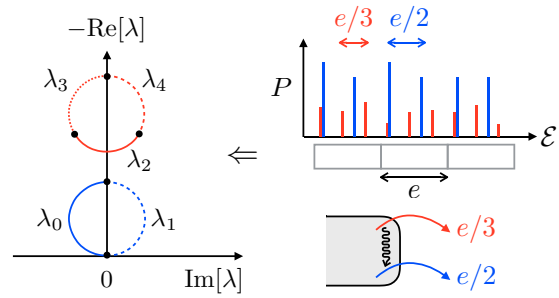

FIG. 6. The analogy between a topological eigenspectrum with broken periodicity, and the transport of (fractional) charges measured with a pixelated detector. On the left-hand side, we show again the generic example of the eigenspectrum of Fig. 1. On the upper right-hand side, we show a pixelated detector setup that gives rise to the spectrum on the left side. Thus, the spectrum on the left is equivalent to the transport of $e/2$ and $e/3$ charges, measured with a detector that has a minimum resolution of the elementary charge e. The fact that one of the bands (the red band with charge $e/3$) is decaying, can be interpreted in simplified terms as an emitter with two possible emission states (see lower right side): the emission state of the $e/3$ band is unstable, eventually decaying to the $e/2$ emission state.

which are measured with a detector that can only resolve the transport in units of the elementary charge e; see Fig. 6. We can think of this transport in terms of the simple picture of an emitter that is either in a state where it emits $e/2$-charges, or in a state that emits $e/3$ charges. The fact that the $e/3$ band is decaying can then, in addition, be regarded as the $e/3$ emission state being unstable, i.e., when the emitter is in this state, it relaxes to the stable $e/2$ emission state with a given rate. Along these lines, we are now also able to understand the third topological phase for the double quantum dot, depicted in Fig. 4(d). Namely, it corresponds to a stable emission state of regular electrons, and an unstable emission state with a fractional charge $e/2$.

To state the above in generalized terms, we find that each band ν, with periodicity p_ν, contributes to the transport with the fractional charge

$$e^*_\nu = \frac{e}{p_\nu}. \tag{27}$$

This is a central result of this paper, establishing the initial claim depicted in Fig. 1.

While we already refer to the eigenmodes as contributions with a fractional charge, we would like to concretely ask the question, to which extent can we think of these eigenmodes as fractionally charged *quasiparticles* in a similar sense to the excitations appearing in Luttinger liquids or the FQHE. We can provide two arguments in favour of such an interpretation. First, through the previous procedure we can draw a straightforward correspondance from topologically nontrivial FCS in sequential tunneling to an auxiliary system which contains excitations described by a charge operator with fractional eigenvalues, e^*_ν. This auxiliary system is only physical, if we requantize its charge by invoking the notion of a minimal detector resolution of size e. Of course, these fractionally charged quasiparticles are thus fictitious, because the addition of a detector with finite resolution is mandatory. But, as we

have already stressed on several occasions, a similar requantization of charge is necessary also for strongly correlated systems. Note importantly, that integer charge eigenvalues are not only a necessity for the total charge of a system, but also of its subparts, *if* the charge of such a subpart is directly measured. Therefore, from this transport measurement perspective, we find no compelling reason why this notion of fractionally charged quasiparticles should be more or less fictitious than the one of quasiparticles in strongly correlated systems, since charge quantization in units of e is fundamental for *any* electronic system.

This leads us to the second argument. Namely, we want to point out a possible relation of the previously introduced detector resolution to the reintroduction of integer charge quantization in Luttinger liquid theory, as it was proposed in Ref. [14]. To briefly repeat, we pointed out in Sec. II C that Gutman *et al.* [14] propose to reintroduce charge quantization into Luttinger liquid theory by simply accepting the values of the moment generating function only for χ from $-\pi$ to π, and continuing the function periodically beyond that interval. We could alternatively reintroduce charge quantization in their result through adding a finite detector resolution of e, along the lines presented above. In fact, this procedure provides a similar result as the one in Ref. [14] except that it does not simply discard the values of the moment generating function beyond the interval $[-\pi, \pi]$. Instead, due to the copying of eigenvalues described above, these values would be folded back onto the interval between $-\pi$ and π, as decaying modes, such that the interval $-\pi < \chi < \pi$ can be considered as a Brillouin zone (again with χ being a detector momentum) with a unit cell size given by e (or more precisely $1/e$). For finite times, the two procedures provide a moment generating function with the same lowest mode, but our procedure gives rise to additional extra modes which decay exponentially with time. For long times, the two results eventually converge, where the decaying bands no longer contribute. We emphasize that at this point, both methods to enforce a 2π-periodicity are completely *ad hoc*, and we cannot say which of the two, if any, can be formally justified, as such an effort would go way beyond this work. We are not aware of generalizations of Luttinger liquid theory taking into account the issue of integer charge quantization [72,73]. We emphasize though that later in this work, in Sec. III B, we consider the special case of superconducting transport across Josephson junctions. Here the 2π-periodicity, and thus the charge quantization in terms of multiples of e (in fact, it will be multiples of $2e$, since we will consider supercurrents), can be justified on formal grounds, even in the presence of strong correlations. This allows us to formulate an even closer analogy.

To conclude, the ramifications of our result may well be, that transport statistics generally turn out to be an ill-suited observable to unequivocally identify exotic quasiparticles, such as Laughlin quasiparticles, or parafermions. At the very least in the here considered low-frequency regime of FCS, based on the topological arguments presented above, we do not see any qualitative feature which would distinguish them from the fractional effect in sequential tunneling. More research will be required to definitively answer this question, e.g., by a better understanding of charge quantization in Luttinger liquid theory, or by comparing topological features in the high-frequency transport statistics.

Finally, we stress that surprisingly, the pixelation of the detector as described above does not actually lead to a loss of information about the detector dynamics: the eigenvalues $\lambda_\nu(\chi)$ are still exactly observable even when the detector has insufficient resolution. We will provide a concrete example within the context of quantum transport, where this principle can be exploited (see Sec. IV D). Finally, we note that we have so far included only charges that are rational fractions of e. The more general case when e and e^* are incommensurable, may be interesting for several reasons, such as to strengthen the analogy to Luttinger liquids (where quasiparticles with irrational fractions are possible), or also in the context of measuring beyond the detector resolution.

III. NONEQUILIBRIUM GEOMETRIC PHASES AND ANALOGY TO FRACTIONAL JOSEPHSON-EFFECT

In previous sections, we have emphasized the nontrivial relation between fractional charges, related to the periodicity of the eigenspectrum, and integer charge quantization, embedded in the global periodicity of the moment generating function m, and consequently, of the kernel W. For the particular example of sequential electron tunneling through quantum dots, we have seen that the braid phase transition arises from transport being measured locally, at a sharp interface, missing certain tunneling events. Moreover, we were able to relate this principle to a general notion of a detector with a finite resolution (given by the integer charge) and a discrete process with a subresolution size (the fractional charge). We will show in this section that there arises a nontrivially quantized geometric phase, due to the mismatch between the two. In fact, this geometric phase contains additional information beyond the topology of the eigenvalues: Namely, it is nontrivial only when the periodicity of the eigenspectrum is *different* from the periodicity of the kernel W, thus explicitly relating the former with the latter.

Importantly, by means of this geometric phase, we will show subsequently that the charge fractionalization in sequential electron transport can be considered as a classical analogy to the fractional Josephson effect, emerging in topological Josephson junctions [37–43].

We note that while topological invariants defined through geometric phases in parallel vector transport are well-established in the context of *closed* topological quantum systems, their generalization to *open* quantum systems is still an actively considered, open problem [28–36,93–97]. Our work contributes to the search for appropriate geometric phases in open quantum systems, by proposing a phase defined through the detector degrees of freedom.

A. Relation between geometric phase and fractional charge

Let us begin by defining the geometric phase, where we first only deal with the mathematical framework, and explain later in Sec. IV C, how such a vector transport can be measured physically. The geometric phase of interest arises, when performing a parallel vector transport of $|n(\chi))$ along χ. The parallel vector transport can be conveniently implemented

through a discretization. We take the projector $|n(\chi))(n(\chi)|$ at a certain χ_0 and repeatedly apply it to itself for increasing $\chi_j = j\Delta\chi + \chi_0$, for the integer j going from 0 to J. Going to the continuum limit $\Delta\chi \to 0$, $J \to \infty$ (while keeping $\chi_J = J\Delta\chi$ finite) and taking the trace of the resulting matrix object, we receive a phase factor times an overlap function

$$\lim_{\Delta\chi\to 0} \mathrm{tr}\left[\prod_{j=0}^{J} |n(\chi_j))(n(\chi_j)|\right] = e^{-\int_{\chi_0}^{\chi_J} d\chi (n(\chi)|\partial_\chi|n(\chi))} (n(\chi_0)|n(\chi_J)). \tag{28}$$

This quantity is manifestly gauge invariant, in the sense that we can transform $|n(\chi)) \to \alpha(\chi)|n(\chi))$ and $(n(\chi)| \to \alpha^{-1}(\chi)(n(\chi)|$ with an arbitrary, differentiable complex function $\alpha(\chi)$, as long as α is invertible for all χ. If we want to completely isolate the phase factor, and get rid of the overlap function $(n(\chi_0)|n(\chi_J))$, then we need to continue our path in χ until we end up in the same eigenvector as the initial one. For a generally topological eigenspectrum, this means that we may need to advance χ by more than just 2π. In fact (and as already stated in Sec. II B) due to the 2π-periodic $W(\chi)$, both the eigenvalues and eigenvectors have the same redundancy, such that we may likewise switch to the reduced band index ν for the geometric phases. Choosing a $2\pi p_\nu$-periodic gauge for the eigenvectors, and setting the initial $\chi_0 = 0$ (without loss of generality) we may relate Eq. (28) to the geometric phase

$$\mathcal{B}_\nu = e^{-\int_0^{2\pi p_\nu} d\chi (\nu(\chi)|\partial_\chi|\nu(\chi))}. \tag{29}$$

First of all, let us verify that this actually corresponds to a real phase, that is, $i\int_0^{2\pi p_\nu} d\chi (\nu(\chi)|\partial_\chi|\nu(\chi)) \in \mathbb{R}$. In fact this is ensured by the symmetry $W^*(\chi) = W(-\chi)$, which originates from the fact that all transition rates in W are real. As long as we follow bands with $\lambda_\nu^*(\chi) = \lambda_\nu^*(-\chi)$, it follows likewise that the geometric phase is real [98].

Now we investigate the connection between the geometric phases and the braid topology. Crucially, while the geometric phases for individual bands are, in general, not quantized, we can show that their product is. Namely, we can demonstrate that for a quite general kernel $W(\chi)$ (we will elaborate in a moment, how general),

$$\mathcal{Z} = \prod_\nu \mathcal{B}_\nu = \prod_\nu (-1)^{p_\nu - 1} = \prod_\nu (-1)^{e/e_\nu^* - 1}. \tag{30}$$

Due to $e/e_\nu^* = p_\nu \in \mathbb{N}$, $\mathcal{Z}$ is manifestly $= \pm 1$. This product of geometric phases thus directly depends on the ratios of the periodicity of the eigenspectrum *with respect* to the periodicity of $W(\chi)$ itself, indicating the mismatch of the fractional charges e_ν^* of the quasiparticles with the integer charge quantization e (i.e., the detector resolution). Importantly, the eigenvalues themselves do not contain the information of the periodicity of $W(\chi)$, which is why $\mathcal{Z}$ carries additional information specific about the detector. This is a further main result of this paper. Let us stress, in addition, the importance of taking into account the redundancy of bands. Had we defined $\mathcal{Z}$ through the product of n instead of ν, it would always be trivially $+1$, independent of the topology.

The full derivation of Eq. (30) is detailed Sec. S2.4 in the Supplemental Material [74]. We here briefly recapitulate the main steps and assumptions to demonstrate the quantization of $\mathcal{Z}$. The chief requirement for deriving Eq. (30) is that $W(\chi)$ can be decomposed into the form $W(\chi) = \sum_N e^{i\chi N} W_N$, that is, a kernel that describes the statistics of some discrete process. The proof then involves a generalization to complex counting fields $\to \chi \in \mathbb{C}$. As we already stated in Sec. II B, in this complex space, we find that $W(\chi)$ exhibits isolated points, so-called exceptional points, where W has no longer well-defined left and right eigenvectors. To each exceptional point one can associate a braid generator (along the lines of Artins braid theory [84]). As far as the geometric phase is concerned, the integrals in Eq. (30) can be reduced into a sum of integrals which enclose only the individual exceptional points (due to the integrals being analytic everywhere else). We then find that each exceptional point contributes a phase $e^{i\pi} = -1$ to the total phase. This particular step is in accordance with a similar result found in Ref. [32]. The final step then involves relating the periodicities p_ν of the eigenspectrum to the number of exceptional points enclosed by the contour of real χ, leading eventually to Eq. (30). In fact, based on the analysis by means of exceptional points, the number $\mathcal{Z}$ can be understood as an element of the $\mathbb{Z}_2$-group, where the nontrivial group operation is associated to moving an exceptional point across the real χ line. Consequently, two distinct topological phases with the same $\mathcal{Z}$ are, in general, separated by another phase with $-\mathcal{Z}$.

Apart from indicating the mismatch between fractional charges and integer charge quantization, Eq. (30) also emphasizes the importance of measuring at a sharp interface. As a reminder, in Sec. II B we introduced the notion of spatially imprecise detectors, described by kernels of the form $e^{i\chi\hat{n}p} W(\chi) e^{-i\chi\hat{n}p}$, where measurements at the left and right interface occur with a probability of p and $1-p$, respectively. Such kernels are no longer 2π-periodic, and thus violate the assumptions to derive Eq. (30). Indeed, while this unitary transformation leaves the eigenvalues invariant due to current conservation (as we already stated), it should become clear now that the geometric phases are affected by it, as they depend on the eigenvectors. In particular, for an arbitrary $p \in \mathbb{R}$, the kernel is not even periodic anymore, since the probabilities to measure from the left (p) and to the right contact ($1-p$) are incommensurable. Here, due to the incommensurability a meaningful geometric phase could only be defined by extending the system to two explicit counting fields, one on the left and one on the right, and we expect that we would have to consider generalizations of a 2D Chern number instead of the 1D geometric phase (in fact, to some extent similarly in spirit to Ref. [99] where the incommensurability of two frequencies in time space is exploited). Such considerations of two-terminal measurements go beyond the scope here, and will be considered in the future. To sum up, we can only guarantee that $\mathcal{Z}$ is a meaningful topological number, when there is a local, sharp measurement at exactly one reservoir. This shows that $\mathcal{Z}$ is highly sensitive to how the transport is physically measured. This dependence on where a transport measurement occurs will again become important in the subsequent Sec. III B, where we explain the analogy to the fractional Josephson effect.

We now relate the previous geometric phase defined in the detector space to some of the other recent efforts to generalize

geometric phases to open quantum systems. For instance, the body of work elaborated in Refs. [28,29,34,97] strives to understand the topological structure of *open* quantum systems in terms of geometric phases related to the density matrix. In particular, in Ref. [34] 1D open quantum systems with a momentumlike degree of freedom k are studied. The authors define a geometric phase based on a many-body correlation function, which, in the thermodynamic limit, returns the standard Zak phase of the ground state in spite being at finite temperatures. A relation to the geometric phase defined in this paper can be found in so far as χ can be considered as a detector momentum, i.e., the conjugate variable to the number of transported electrons. However, the geometric phase that we propose is a genuine nonequilibrium quantity, and it is, in general, difficult to relate the connection $\sim(\nu|\partial_\chi|\nu)$ to the eigenvectors of a closed system and thus to the standard Zak phase.

A closer relation exists with respect to geometric phases emerging in the FCS of time-dependently driven quantum pumps [93–96,100,101]. Further works by Refs. [30,31] elaborated that the pumping geometric phase is related to the gauge degree of freedom arising from calibrating the transport detector. The time-dependent driving manifests in an explicit time-dependence of the kernel $W_t(\chi)$. The resulting pumping geometric phase, $\sim(\nu(\chi)|\partial_t|\nu(\chi))$ (also referred to as the Nemenman-Sinitsyn phase), provides the lowest order correction of the stationary contribution to the FCS, due to nearly adiabatic driving. Importantly, the difference to our approach is, that we perform a parallel vector transport not along some pumping parameters, but along the counting field itself, $\sim(\nu(\chi)|\partial_\chi|\nu(\chi))$. In essence, instead of a time-dependent driving, we here have to invoke the notion of a time-dependent measurement of the FCS. We will elaborate on this in more detail in Sec. IV C, where we examine strategies to measure $\mathcal{Z}$ experimentally.

There is, however, one important difference between the pumping geometric phase $(\nu(\chi)|\partial_t|\nu(\chi))$ and the one we propose in Eq. (29). The difference has to do with the unitary transformations of the form $e^{i\chi\hat{n}_p}W(\chi)e^{-i\chi\hat{n}_p}$, as discussed above. Namely, while $\mathcal{B}_\nu$ is sensitive to such transformations, the pumping geometric phase is not. This is easily explained through the role of current conservation, as it has been introduced in Sec. II B. Namely, as just stated, the phase $\mathcal{B}_\nu$ can only be accessed through time-dependent measurements, where displacement currents cannot, in general, be neglected. The pumping geometric phase, however, includes merely time-dependent driving, but no time-dependent counting fields. Therefore, the pumping geometric phase represents only the measurement of dc currents. And importantly, in the dc limit, any displacement currents vanish, hence, it does not matter whether we measure the current entering the quantum system through one reservoir, or the one leaving the system into the other reservoir. The role of current conservation will again be of importance in the now following section, when discussing the fractional Josephson effect.

B. Analogy to fractional Josephson effect

Here we compare the fractional effect in sequential electron tunneling to the fractional Josephson effect. Apart from the surprising fact that such a comparison is even possible, in general, we have one more important motivation. Namely, as we mentioned in Sec. II D, we expect a proper requantization of charge to be nontrivial for Luttinger liquid theory. Therefore, an unambiguous comparison of the fractional nature of charges in the two systems, beyond the *ad hoc* arguments presented previously, seems out of reach. However, as we will show now, in the case of superconducting transport across Josephson junctions, we can propose measurement schemes that preserve some form of charge quantization. Based on this, we can show that also here, the mismatch between the quasiparticle charge and the detector resolution limit, leads to the same measurable effect: a nontrivially quantized geometric phase.

To begin, let us note that in superconducting junctions, the number $\mathcal{N}$ of coherently transported Cooper pairs across the two superconductors has likewise its conjugate pendant in the form of the phase difference ϕ. In fact, we can think of the pair N and χ describing dissipative transport as the classical components of the quantum variables $\mathcal{N}$ and ϕ. In particular, just as a 2π-periodicity in χ indicates that the electron is the fundamental unit of dissipative electron transport, a 2π-periodicity in ϕ corresponds to the Cooper pair being the underlying unit in which a supercurrent is mediated. However, excitations carrying a fractional Cooper pair charge can appear in junctions with topological superconductors [37,41–43,102]. And once more, we need to define exactly, how such fractional charges are defined and measured. The subgap transport physics of such junctions can be described by a Hamiltonian operator, $H_{\rm sub}(\phi)$, valid for energies $< \Delta$, where Δ is the superconducting gap. Hence, very similarly to sequential electron tunneling, the transport can be described in terms of a linear operator along a transport degree of freedom (ϕ). This Hamiltonian may likewise give rise to an eigenenergy spectrum with broken periodicity in ϕ, either a 4π-Josephson effect for Majorana fermions with half a Cooper pair charge [37], or an 8π-Josephson effect for parafermion transport, carrying a quarter of the Cooper pair charge [41]. However, yet again, care has to be taken as far as the periodicity of the Hamiltonian itself is concerned. Namely, the periodicity of the Hamiltonian is *not* given by the charge of the underlying quasiparticle or edge state, but (similar to above) by a transport *detector*—and that the periodicity of $H_{\rm sub}$ has measurable consequences in the geometric phase defined along ϕ. For instance, if an experimenter performs a subgap transport measurement that couples to the integer number of transferred Cooper pairs, $H_{\rm sub}$ will remain 2π-periodic, such that, the periodicity of the underlying spectrum is broken *with respect to* the Hamiltonian.

To visualize this at an example, let us consider the Hamiltonian put forth by Fu and Kane [37]. The model is a quantum spin Hall insulator (QSHI) proximitized by ordinary s-wave superconductors, separated by a small nonproximitized patch, in the interval $0 < x < L$,

$$\mathcal{H} = -iv_F\sigma_z\tau_z\partial_x - \mu\tau_z + M(x)\sigma_x + \Delta\theta(-x)\tau_x + \Delta\theta(x-L)e^{i\phi\tau_z}\tau_x, \tag{31}$$

where σ_i and τ_i denote the left and right mover space of the QSHI edge states and the Nambu space, respectively. The

induced gap is referred to as Δ. The term proportional to $M(x)$ has a finite support only within the interval $0 < x < L$ and denotes a magnetic impurity which allows the spin-locked edge states to scatter. Note that $\mathcal{H}$ describes the interplay of a single electron and a single hole. The full many body representation of the system can be obtained through $H = \frac{1}{2}\Psi^\dagger \mathcal{H} \Psi$ (see also Ref. [37]), where the field operator $\Psi = (\psi_+, \psi_-, \psi_-^\dagger, -\psi_+^\dagger)$ is composed of the fields of left $(-)$ and right $(+)$ moving electrons and holes. Note that already on this general level, the Hamiltonian is 2π-periodic by construction, since the phase ϕ is explicitly attached to one of the two superconductors. We will elaborate on the justification of this choice in a moment.

Let us focus on the supercurrents at very low temperatures (and neglect quasiparticle contributions). In this regime, one can derive a Hamiltonian describing the subgap physics only. While Fu and Kane themselves already provided such a Hamiltonian in the many-body basis of the Majorana fermions [37], we here rederive it in the basis of outcoming electrons and holes (starting from Beenakker's formula [103], see Sec. S3 in the Supplemental Material [74]) because this later basis facilitates the comparison to the kernels $W(\chi)$. We find

$$\mathcal{H}_{\text{sub}}(\phi) = \frac{\Delta}{2}\begin{pmatrix} 0 & t_e[1+e^{i\phi}] \\ t_e^*[1+e^{-i\phi}] & 0 \end{pmatrix}. \tag{32}$$

For this Hamiltonian we find the eigenspectrum $\epsilon_\pm(\chi) = \pm\Delta|t_e|^2\cos(\phi/2)$ in accordance with Ref. [37]. Obviously, the eigenspectrum has a broken periodicity with respect to the Hamiltonian in Eq. (32). However, as of right now, the 2π-periodicity in $\mathcal{H}$ (and consequently in $\mathcal{H}_{\text{sub}}$) appears essentially by construction, as the phase is attached to only one of the superconducting contacts. We could also construct different representations for $\mathcal{H}$, respectively, $\mathcal{H}_{\text{sub}}$, for instance, with $\Delta e^{-i\phi/2}$ on the left and $\Delta e^{i\phi/2}$ on the right, or any other combination. In fact, by inspecting the form of the Hamiltonian in Eq. (32), we see that the different choices are related by the same unitary transformations as we discussed them for the kernel W in previous sections (see Secs. II B and III A). Importantly, per se, all of these choices are, of course, physically valid. However, we have to note that when performing a parallel vector transport along ϕ, e.g., through making ϕ time-dependent, the geometric phase picked up differs for different choices. And this geometric phase, which is a 1D Zak phase, is gauge invariant [see Eq. (28)] and therefore measurable. Consequently, the different choices of where the phase difference ϕ drops must express physically different situations, as we explain now.

First, let us show how we can implement the 2π-periodic $\mathcal{H}$. For this purpose, let us consider an open circuit geometry [104], and apply a bias V between the topological material and one s-wave superconductor [see Fig. 7(a)]. In this case, we find that $\to \Delta e^{i\phi(t)}$, where $\dot{\phi}(t) = 2eV$. Here, $\phi(t)$ couples to the Cooper pairs transported into and out of the biased superconducting contact. Consequently, the relevant unit of transport which is probed is the *integer* number of Cooper pairs that arrive at the biased contact. We can consider this as a fixing of the resolution of our detector to $2e$. In this case, the charge transferred through the Majorana states, e, is in mismatch with respect to the underlying Cooper pair charge in the s-wave contact. Here, we find that the geometric

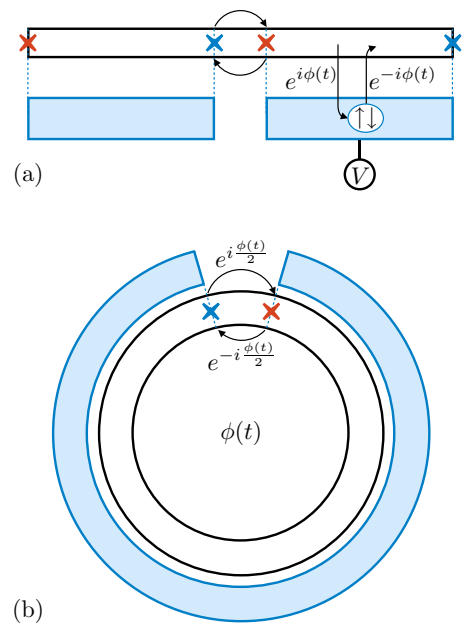

FIG. 7. (a) Sketch of the open circuit geometry of a topological Josephson junction. The Majorana fermion edge states are depicted with blue and red crosses. The superconductivity is induced by the s-wave superconducting contacts (light blue). In this circuit, a bias V is applied between the topological material and the s-wave superconductor, such that the phase $\phi(t)$ couples to the Cooper pairs leaving and entering the contact. (b) Sketch of the closed circuit geometry. Here, a time-dependent ϕ can be realized through a time-dependent magnetic field threading the loop. The phase $\phi(t)/2$ couples to individual Majorana fermions tunneling across the junction.

phase picked up, when going from $\phi = 0$ to 4π is equal to -1 (similarly to the single level quantum dot in the topological regime).

We can contrast this to a different, closed circuit geometry, see Fig. 7(b), where a bias can obviously not be applied. We can, however, implement a time-dependent $\phi(t)$ by ramping up a magnetic field threading the loop. In this case, we have a slightly different starting Hamiltonian,

$$\begin{aligned}\mathcal{H}' = &-iv_F\sigma_z\tau_z\partial_x - \mu\tau_z + M(x)\sigma_x \\ &- v\sigma_z eA(x) + \Delta\theta(-x)\tau_x + \Delta\theta(x-L)\tau_x,\end{aligned} \tag{33}$$

where $A(x)$ has a finite support only for $0 < x < L$, and $2e\int_0^L dx A(x) = \phi$. In the short junction limit, $L \to 0^+$ (where the phase drops sharply across the junction), we can easily see that $\mathcal{H}$ and $\mathcal{H}'$ are related through the unitary transformation $U^\dagger \mathcal{H} U = \mathcal{H}'$, with $U = e^{-i\theta(x)\frac{\phi}{2}\tau_z}$. From this transformation it becomes obvious that $\mathcal{H}'$ is 4π-periodic, and it follows that here the geometric phase picked up from 0 to 4π is trivially 1. Physically, we note that here the magnetic field couples to the electrons (and *not* the Cooper pairs) moving to the left (right) through the phase factor $e^{i\phi/2}$ ($e^{-i\phi/2}$), and is therefore able to resolve single charges e.

Importantly, note that the two circuits in Figs. 7(a) and 7(b) not only have a different periodicity in ϕ but also a different many-body spectrum: In the open circuit, the Majorana subspace is doubled, due to the extra edge states appearing at the additional ends (see also, e.g., Ref. [105] and references

therein). We would like to point out, however, that it is not the different many-body spectrum of $H(\phi)$ that is the direct origin of the observable different Zak phase, but really the relative periodicity breaking between the Hamiltonian and its eigenspectrum. This periodicity breaking is already accounted for by $\mathcal{H}$, whereas the field operators Ψ appearing in the full many-body Hamiltonian H do *not* depend on ϕ.

To summarize the above, we can draw the following analogy to the sequential tunneling regime. Namely, in both types of system, the geometric phase picked up along ϕ (respectively, χ) depends on the relationship between the periodicity of the operator describing the dynamics, and the periodicity of the eigenspectrum. And similarly, we can relate the charge of a quasiparticle to the periodicity of the eigenspectrum, and the charge that couples to ϕ (or χ) to the periodicity of H (W), and interpret the latter as a detector resolution.

Crucially, also the underlying origin for the measurable difference for the Hamiltonians with different periodicy is the same as for sequential tunneling. Namely, the invariance of the energy eigenspectrum on the periodicity of $\mathcal{H}$ ($\mathcal{H}_{\text{sub}}$) is likewise based on current conservation. Now, to have access to the geometric phase, we need to vary ϕ in a time-dependent fashion. This is very similar to a parallel vector transport in χ, which necessitates time-dependent counting fields (see Secs. III A and IV C). And as we pointed out already at the end of Sec. III A, when having access to time-dependent transport, displacement currents do have to be taken into account, as the current entering a given system at one end is not necessarily the same as the one exiting at the other. We here see a quantum version of the same principle at work: a time-dependent variation of ϕ leads to measurable differences with respect to the interface at which the time-dependent phase $\phi(t)$ drops. To further corroborate our surprising finding, we note that in a recent work [106] it was very similarly noted that attaching time-dependent phase drops $\phi(t)$ to different parts in the circuit Hamiltonian leads to measurably different results in the observables (in the case of Ref. [106] to different circuit relaxation rates), which have to be derived and interpreted properly.

Importantly, for the open circuit we can immediately generalize our statement to the 8π Josephson effect, which emerges when many-body interactions (in particular, pair-backscattering) are present in the junction. The many-body interactions can be included on the level of Eq. (31) (of course, in the appropriate many-body representation, see Ref. [41]), without changing the periodicity of the Hamiltonian. Thus, we get a 2π-periodic Hamiltonian with an 8π-periodic spectrum, indicating that we need four consecutive parafermion tunneling events to register the transport of one Cooper pair arriving at the biased superconducting contact.

Crucially, once we have a description of the subgap physics through a 2π-periodic operator $H_{\text{sub}}(\phi)$ which is detached from the continuum of states at energies $\geqslant \Delta$ (which is the case for the here considered topological superconducting junctions, see Ref. [41]), the operator $H_{\text{sub}}(\phi)$ fulfils the exact same set of properties as $W(\chi)$, which are needed to compute the product of generalized geometric phases $\mathcal{Z}$ given in Eq. (30), simply by replacing χ with ϕ. Note that this renders our result of $\mathcal{Z}$ very general, as it can describe the topology of the subgap physics of quite generic Hamiltonians H_{sub} (e.g., including many-body interactions), as long as the eigenspectrum is discrete, and detached from the continuum.

Concerning this analogy, there remain two subtle issues to be discussed. The first concerns the closed circuit in Fig. 7(b). As we have seen above for Majorana fermions, the parallel vector transport is here realized through a change of the magnetic field, and leads to a different Zak phase as the open circuit, due to the Hamiltonian being 4π-periodic. Hence, we can find a detector scheme that resolves single electrons (instead of Cooper pairs) tunneling across the junction. This is not surprising, as Cooper pairs are obviously composite particles that can be physically split. However, we expect that the question of how the closed circuit needs to be generalized to the 8π-Josephson effect (including parafermions) becomes highly nontrivial. We remind that the emergence of parafermions require likewise Luttinger liquid physics at the junction, and thus, this question relates back to the problem of properly reintroducing charge quantization in this interacting theory, as we have laid it out at several points in this paper. We expect, relying again on the argument of Gutman *et al.* [14], that if $\phi(t)$ drops across a sharp interface, the 4π periodicity needs to be preserved as the magnetic field cannot fundamentally couple to a charge below the electron charge. However, once more, this question deserves proper attention and goes well beyond the scope of the present work.

The second subtlety is related to the general validity of comparing a nonequilibrium, non-Hermitian system (sequential tunneling), with a Hermitian system (Josephson junction). Namely, while the kernel W has, in general, complex eigenvalues, the spectrum of H_{sub} is, of course, real, since supercurrents are an equilibrium property. Consequently, the connection of the latter to the braid group may not be obvious at first sight. As we show in Sec. S2.3 in [74], the real spectrum with a crossing instead of a braid can be understood as a merging of two exceptional points with equal braid generator. Because the braid generators are equal, they cannot annihilate, and the nontrivial topology, including a nontrivial $\mathcal{Z}$ persists. Therefore, we find the same $\mathcal{Z}$ for topological Josephson junctions, by replacing χ with ϕ. A nontrivial $\mathcal{Z}$ defined along ϕ indicates likewise the transport of a quasiparticle with a fractional Cooper pair charge, measured by a supercurrent mediated in units of integer Cooper pairs. In this sense, the product of geometric phases $\mathcal{Z}$ demonstrates a profound analogy between topological FCS in sequential electron tunneling and the fractional Josephson effect in topological superconducting junctions.

Note, in addition, that for sequential tunneling, no special symmtries are required for the system to be in the topological phase. The only fundamental condition is a nonequilibrium bias, allowing for a complex, braided eigenspectrum, whereas in equilibrium the eigenspectrum of W is real and no braiding can occur, in general, as already pointed out by Ref. [16] and in Sec. II C. Importantly, the same principle also holds for the subgap physics in conventional Josephson junctions, which are described through a generally gapped Hermitian operator H_{sub}. The reason that the periodicity can nonetheless be broken for a Hermitian operator, is due to the presence of *topological* superconducting junctions, where additional symmetries guarantee that the merging of braid generators

remains stable. In the previous example, these symmetries are provided by the topological QSHI weak link (in combination with magnetic impurities for the 4π Josephson effect [37] or the pair-backscattering in the weak link for the 8π effect [41,42]). Therefore, while the fractional effect in the Josephson junction relies on special symmetries, the one in sequential electron tunnling is protected even in the absence of special symmetries, at the expense of rendering the dynamics non-Hermitian (thanks to the nonequilibrium bias).

In fact, this analogy opens up the possibility to simulate the topology of the fractional Josephson-effect by means of regular electron transport. This idea thus falls in line with a number of very recent proposals to implement topological behavior known from the quantum domain through (semi)classical dynamics, most notably the study of geometric and topological effects in the diffusion dynamics of polymers [44,45], or also the implementation of the Su-Schrieffer-Heeger (SSH) model through single electron transistors [46]. In addition, we emphasize that the here proposed simulator is potentially more stable than the fractional Josephson effect itself. In particular, since the Josephson effect relies on Cooper pair physics, it is naturally susceptible to fermion parity breaking due to quasiparticle tunneling [37,47,48]. The incoherent fractional effect, however, as discussed in Sec. II, is *defined* in terms of single electron transport, and thus by nature insensitive to parity breaking.

IV. EXPERIMENTAL VERIFICATIONS AND POSSIBLE APPLICATIONS

We have so far established the general concept of a fractional charge in sequential electron transport and its striking analogy to fractional charges in strongly correlated systems. In the final part of our work, we aim to point towards experimental verifications of our claims. First, we study a nearly Poissonian regime, where a measurement of the lowest few cumulants of the current suffices to determine the fractional charge of the stationary mode, along similar lines as Eq. (3). By means of the topological argument, we show that the shot noise regime in quantum dots, which was hitherto considered as strictly sub-Poissonian [107], should actually be interpreted as a nearly Poissonian transport with a fractional charge. With the continued experimental progress in the detection of higher cumulants of the current [49–59] we believe that the fractional nature of sequential electron transport could be verified with existing technology.

When going beyond this Poissonian regime, and when trying to measure fractional charges of decaying modes, we need to have access to the time-dependent dynamics of the detector. These can be measured by means of the detector's waiting-time distribution, describing the statistics of time intervals between transport events [60–66]. While it is known that the latter provides the eigenmodes, we here show that the waiting times provide also the geometric phases, and thus $\mathcal{Z}$. At the end, we study some realistic cases of detector errors and comment on detector backaction effects. We argue that neither of them can fundamentally hamper the measurement of the topological features. Finally, we will provide a concrete example how the braid phase transition in the FCS can be used to perform measurements beyond the detector resolution limit.

A. Experimental observation of ground-state fractional charge

Let us revisit the single-level quantum dot model from Sec. II C, to propose concrete, feasible experiments to measure the fractional nature of the ground-state charge. As we have already indicated in Sec. II C, the topological phase is favoured when the transport is strongly biased in one direction, e.g., from left to right, i.e., $(\mu_{\rm L}-\epsilon)/k_{\rm B}T \gg 1$ and $(\epsilon-\mu_{\rm R})/k_{\rm B}T \gg 1$ (such that $f_L \to 1$ and $f_R \to 0$). Second, the presence of the fractional charge depends also strongly on the coupling asymmetry. The most stable topological phase is reached for sufficiently symmetric coupling. In the regime of strong bias to the right, symmetric coupling corresponds to $\sigma\Gamma_{\rm L} = \Gamma_{\rm R}$. For strongly asymmetric coupling, however, either $\sigma\Gamma_{\rm L} \ll \Gamma_{\rm R}$ or $\sigma\Gamma_{\rm L} \gg \Gamma_{\rm R}$, the spectrum is always trivial.

Let us here focus on a special regime of highly symmetric coupling. We will see now that the fractional charge is accessible through measuring only the lowest few cumulants. Namely, we find that the cumulant generating function is given as

$$c(\chi) \approx \gamma\left(e^{i\frac{\chi}{2}}-1\right)+\delta\gamma\left(e^{-i\frac{\chi}{2}}-1\right), \tag{34}$$

where the term proportional to $\gamma = (\sigma\Gamma_{\rm L}+\Gamma_{\rm R})/2$ is the leading term, and $\delta\gamma \ll \gamma$ is the lowest order correction. The correction takes into account both small deviations from the exact tunnel coupling symmetry, and small thermal excitations, $f_{\rm L} \approx 1-\delta f_{\rm L}$ and $f_{\rm R} \approx \delta f_{\rm R}$. Taking the sum of these two corrections, we find $\delta\gamma = (\sigma\Gamma_{\rm L}-\Gamma_{\rm R})^2/(8\gamma) + \gamma(\sigma\delta f_{\rm L}+\delta f_{\rm R}/\sigma)/2$. As we see, the statistics given in Eq. (34) results in a nonequilibrium transport statistics of ordinary electrons, which are indistinguishable from an almost Poissonian transport statistics with a fractional charge $e^*/e = 1/2$. The leading term corresponds to the special limit which has already been remarked by Refs. [15,22]. If the corrections were zero, then it would suffice to measure the current $|I| = \frac{e}{2}\gamma$ as well as the noise $S = (\frac{e}{2})^2\gamma$, such that the Fano factor, as introduced in Eq. (3), would provide us with a fractional charge $e^*/e = 1/2$.

In general, however, one cannot avoid having small deviations from this sweet spot of exact symmetry and perfect bias, and second term in Eq. (34) cannot be neglected. Nonetheless, as we have argued at length in Sec. II C, the fractional charge is of topological nature, and thus protected against small perturbations. Therefore, these small deviations from the exact Poissonian limit do not destroy the fractional charge, but simply render the observation of e^*/e less straightforward. To detect it, we need the information of the higher cumulants. From Eq. (34), we find that the relation between the cumulants is

$$\frac{C_{k+1}}{eC_k} \approx \frac{e^*}{e}\left[1-2\frac{\delta\gamma}{\gamma}(-1)^k\right], \tag{35}$$

up to first order in $\delta\gamma$. As we see, we have two independent factors, the fractional charge e^*/e and the correction factor $\delta\gamma/\gamma$. To read them both out, we need to have access to the first, second, and third cumulants, to create two independent ratios. We stress the very different nature of the two factors

in Eq. (35). While e^*/e is given by the topology and is thus precisely $= 1/2$ for a large connected parameter subspace, the factor $\delta\gamma/\gamma$ depends on the device parameters. Importantly, we note that it is, in particular, the connection of the factor e^*/e to the braid phase transition, which was not considered in Refs. [15,22]. We expect it to be possible to test this result experimentally, e.g., through measuring the cumulants for different parameter settings, and thus to demonstrate the topological origin of e^*/e. We are confident that such experiments are within reach [49–58].

We further note for the sake of completeness that in principle, the first term proportional to γ would contain a renormalization of the same order as $\delta\gamma$. This correction is, however, irrelevant when computing the respective ratios of the cumulants, as in Eq. (35), which is why we discarded it.

Finally, let us point out that a similar regime can be reached for the double quantum dot level; see Fig. 4. For $f_L \approx 1$, $f_R \approx 0$, $f(\epsilon_R - \epsilon_L) \approx 1$, and $\sigma\Gamma_L \approx \Gamma_{LR} \approx \Gamma_R$, we get a regime of Poissonian transport with a fractional charge $e/3$.

Beyond this long-time Poissonian regime, the measurement of e_0^* can in principle still be done by going to arbitrary high cumulants. However, this fact ultimately renders the extraction of the topological factor more and more unpractical by the above method. Moreover, for long measurement times, the decaying bands are suppressed. In the section that follows now, we will show how to measure ground-state fractional charges beyond the Poissonian regime, as well as the fractional charges associated to higher, decaying bands.

B. Waiting-time distribution and topology

In the existing literature, only indirect observations of topological transitions in the FCS have been studied. As we already stated earlier, in the limit of long measurement times, $\tau \to \infty$, the moment generating function for the long-time limit, as defined, e.g., in Eq. (14), is globally discontinuous in the topological phase. The probing of nonanalytic behaviour of the cumulant generating function has been theoretically studied in Refs. [70,71,108] and experimentally verified in Ref. [59]. Here, the nonanalytic behaviour in c manifests as dynamical Lee-Yang zeros, and their location can be extracted from a finite (short) time measurement of high cumulants. Discontinuities in the cumulant generating function do, however, not unequivocally probe a broken periodicity. First of all, note that no actual braid phase transition is required for Lee-Yang zeros to occur, see, e.g., Ref. [70], where very different models were considered with a c that is continuous with a discontinuous first derivative. Within the specific context of sequential electron transport, we can consider another simple generic example: imagine two eigenmodes that do neither cross nor braid in the complex plane, but where, within some connected region in χ, the real parts of the two eigenvalues change their order. At the points where the crossing appears, c is consequently discontinuous even in the absence of a braid topology. Second, even if the nonanalytic behavior indeed stems from a nontrivial eigenspectrum, the mere presence of the discontinuity does not allow us to extract the *periodicity* of the eigenspectrum. Nor does it provide information about the decaying modes which may have a nontrivial charge of their own, as we have elaborated in the previous sections. Therefore we conclude, that to measure fractional charges, be it for the stationary or decaying modes, we need the explicit information of the eigenmodes of the detector dynamics.

As was shown in Ref. [61], the eigenspectrum of $W(\chi)$ is accessible through the waiting-time distribution of the detector, when recording single tunneling events. For the sake of completeness, we here briefly reiterate the main points. In a first step, to simplify the discussion, we limit our consideration to kernels that can be expressed as $W(\chi) = W_0 + e^{i\chi}W_{+1} + e^{-i\chi}W_{-1}$. This form is sufficient to fully describe sequential electron tunneling. Next, we suppose that the parts of the kernel which give rise to transport can be written as products of vectors $W_{+1} = w_+|+)(+|$ and $W_{-1} = w_-|-)(-|$. The vector $|+)$ ($|-)$) is the state the system is in immediately after a "click" of the detector which increases (decreases) the detector state by one. Note that these states do not have to be pure states. The maps $(+|$, $(-|$ trace out all the states the system can be in prior to the corresponding click, weighted with the appropriate probability. Note that, in general, $(+| \neq |+)^T$, $(-| \neq |-)^T$. The *experimentally measurable* quantities are then the probabilities that time τ passes between the events i and j, $(i|e^{W_0\tau}|j)$, where the indices can be $i, j \in \{0, +, -\}$. For instance, $(\pm|e^{W_0\tau}|0)$ is the probability that time τ passes for the first click (either $+$ or $-$) to occur, when starting out in the stationary state. Similarly, $(+|e^{W_0\tau}|+)$ is the probability that time τ has elapsed between two $+$ clicks, without any other click occurring in between. Independently, one has to measure the rates $w_\pm$ at which such clicks occur. Beyond that, no further experimental input will be needed to compute the desired quantities, as we show in the remainder of this work.

Now we can formulate the time evolution of the system-detector dynamics as follows. We start from the full time evolution of the correlator,

$$G_{ij}(\tau) = w_i(i|e^{W(\chi)\tau}|j), \tag{36}$$

with $w_0 = 1$. Expanding the time evolution in orders of $w_\pm$, we arrive at a Dyson-like equation of the form

$$G_{ij}(\tau) = g_{ij}(\tau) + e^{i\chi}\sum_{k=\pm}\int_0^\tau dt\, g_{ik}(\tau - t)G_{kj}(t), \tag{37}$$

where the events that change the detector state correspond to the vortices with the $e^{\pm i\chi}$ prefactors. The free correlator functions $g_{ij}(t) = w_i(i|e^{W_0 t}|j)$ are referred to as the waiting-time distributions, again with $i, j \in \{0, +, -\}$.

Within this framework, the moment and cumulant generating functions are computed through $m(\chi, \tau) = e^{c(\chi,\tau)\tau} = G_{00}(\tau)$. In fact, to extract the eigenvalues $\lambda_n(\chi)$, it suffices to perform a transformation into Laplace space, $g_{ij}(z) = \int_0^\infty d\tau e^{-z\tau} g_{ij}(\tau)$, and solving Eq. (37) provides the condition

$$\det\left[\begin{pmatrix} g_{++}(z) & g_{+-}(z) \\ g_{-+}(z) & g_{--}(z)\end{pmatrix}^{-1} - \begin{pmatrix} e^{i\chi} & 0 \\ 0 & e^{-i\chi}\end{pmatrix}\right] = 0. \tag{38}$$

The set of z which satisfies this condition corresponds to the eigenspectrum $\{\lambda_n(\chi)\}$. That is, once the waiting-time distribution, in form of the correlators g_{ij}, is measured and analyzed in Laplace space, we have access to the full spectrum and its topology, including the information of the charge. Of course, one remaining challenge is the proposition of feasible

experimental setups to actually measure the individual transport clicks. We will present some ideas in Sec. IV C 2.

Finally, we note that to efficiently solve Eq. (38), we can use the fact that W_0 has an eigendecomposition of its own, such that $g_{ij}(t) = \sum_n g_{ij,n} e^{l_n t}$, where $\{l_n\}$ is the eigenspectrum of W_0. It then follows that $g_{ij}(z) = \sum_n g_{ij,n}(z - l_n)^{-1}$, and consequently, solving Eq. (38), eventually simplifies to finding the zeros of a polynomial. On a practical side, fitting the experimentally observed $g_{ij}(t)$ by a sum of exponentials will necessarily come with errors. As long as these errors are small, they cannot pose a serious threat to the correct observation of the topology. We will elaborate on this with more detail as soon as we propose explicit experimental examples, again, see Sec. II D.

For completeness, let us also mention a different method to measure the transport statistics of higher bands, proposed in Ref. [109]. In essence, the authors showed that the long-time cumulant generating function, $c(\chi, \infty) = \lambda_0(\chi)$, can be used to infer the $\lambda_{n>0}(\chi)$ by means of generalized factorial cumulants. This method could therefore potentially be used to measure charges of the higher, decaying bands. However, we expect that we would yet again be limited to the nearly Poissonian regime of fractional transport. Moreover, we see no obvious path toward finding the geometric phases of Eq. (30). This is why we do not consider it in detail in this paper. As we show now, the waiting times, however, *can* provide said geometric phases.

C. Accessing geometric phases through waiting-time distribution

Crucially, as indicated above, with the information provided by the waiting-time distribution, we can not only extract the *eigenvalues* of $W(\chi)$, but also the geometric properties of the *eigenvectors*. Since geometric phases defined along the counting field may be a rather new and perhaps a bit of an unusual proposition, we carefully explain the proposed measurement concept, first generally, and subsequently at an explicit example.

1. The general principle

To see that the waiting times implicitly contain the information of the geometric phases, it is important to realize that within the framework of waiting times, Eq. (37), the counting field χ enters simply as an external parameter. The actual, experimentally measured input is captured in the functions $g_{ij}(t)$. That means, we can modify χ at will, including replacing it with a time-dependent function of the form $\chi \to \omega t$. We thus realize a time-dependent parallel vector transport along χ-space. Performing an adiabatic expansion of any $G_{ij}(\tau)$, we find

$$G_{ij}(\tau) = \sum_n e^{\int_0^\tau dt\left[\lambda_{n,t} - (n_t|\partial_t|n_t)\right]} (i|n_\tau)\,(n_0|j) + \mathcal{O}\left[\frac{\|\omega\|}{\|\lambda\|}\right], \quad (39)$$

where the generalized geometric phase $\int_0^\tau dt\,(n_t|\partial_t|n_t)$ appears, and the expansion parameter $\|\omega\|/\|\lambda\|$ is composed of the ratio between a driving rate $\|\omega\| \sim |(n_t|\partial_t|n_t')|$ and a rate associated to the gap between eigenstates, $\|\lambda\| \sim |\lambda_{n,t} - \lambda_{n',t}|$, for $n' \neq n$. Equation (39) can be derived, starting from Eq. (36), along similar lines as in Ref. [110]. A straightforward derivation can be done when discretizing time space; in fact, Eq. (28) already provides the geometric part of Eq. (39). The additional dynamic prefactor $e^{\int_0^\tau dt\lambda_{n,t}}$ appears because the time evolution of G_{ij} is generated by the full $W(\chi)$, see Eq. (36). Equation (39) demonstrates that we can access the information about geometric phases by means of the correlators g_{ij}, importantly *not* requiring any additional effort on the experimental side.

As we have pointed out in Sec. III A, to extract the geometric phase from Eq. (39), we need to close the path in χ. To repeat, for an eigenspectrum with broken 2π-periodicity, this means that for a given eigenvalue n, we set $\tau_n = \frac{2\pi}{\omega} p_n$, such that we return to the original eigenvector, $|n_{\tau_n}) = |n_0)$, and in this way, we receive the phase $e^{-\int_0^{\tau_n} dt(n_t|\partial_t|n_t)} = e^{-\int_0^{2\pi p_n} d\chi(n(\chi)|\partial_\chi|n(\chi))}$. Due to the already discussed redundancy, we change to the notation of the index of *independent* bands, ν. The determination of the geometric phases and the topological number $\mathcal{Z}$, Eq. (30), is then straightforward. Since we have the entire information of the different g_{ij} at disposal, we can compute the full eigenspectrum $\lambda_\nu(\chi)$ for all χ. Based on this information, we can identify the individual contributions corresponding to a mode n (respectively, ν) in the sum of Eq. (39). Finally, we can eliminate the overlap functions $(i|n_\tau)(n_0|j)$ by dividing $G_{ij}(2\pi p_\nu/\omega)$ with $G_{ij}(0)$. According to Eq. (30) the output from each mode ν is then multiplied. This procedure will be explicitly worked out at an example in the following section.

But before that, let us explain in more detail the notion of a time-dependent counting field. Time-independent counting fields provide the *time-averaged* current statistics. Time-dependent counting fields, $\chi \to \chi(t)$, formally give access to *time-resolved* statistics [111]. To obtain information about a current measurement at a given time t, one applies the functional derivative $\delta/\delta\chi(t)$ to the cumulant generating function. In this sense, in the standard framework of time-resolved statistics, $\chi(t)$ is not actually a mere function of t. Rather it is an assignment of a *different* counting field to each instance in time t. To extract the geometric phase as proposed above, we implement exactly this extra ingredient: With the above procedure, we essentially measure the transport at each time t, and then assign a specific value for $\chi(t)$, $\chi \to \omega t$. The function G_{ij} can then be viewed as a correlation of all measurements with this specific assignment. Thus the here proposed procedure corresponds to a *post-processing* of the transport information we obtained through the measurement of the waiting-time distribution, which is specifically designed to provide us with the generalized geometric phase appearing in Eq. (39).

Let us note a final crucial point. As we indicated, the derivation of Eq. (39) is done in analogy to Ref. [110], which treats geometric phases in closed systems. However, there is an important difference to the open system with a non-Hermitian matrix $W(\chi)$, which renders the extraction of the geometric phase from the previous equation a bit harder. The issue is, that even though ω can always be chosen sufficiently small such that the expansion parameter $\|\omega\|/\|\lambda\|$ is $\ll 1$ (provided that the spectrum is always gapped), nonadiabatic correction can nonetheless become important, due to the prefactor $e^{\int_0^\tau dt\lambda_{n,t}}$, or more specifically due to the eigenvalues λ_n having a nonpositive real part.

This fact becomes evident when considering the following. Suppose we start the time evolution at time $t = 0$ in the stationary state $|0(\chi = 0)\rangle$. As time progresses, the dynamics stays mostly in the corresponding eigenvector $|0(\omega t)\rangle$, apart from some small errors. If, however, the spectrum is nontrivial, then there will come the moment where another eigenvector, say $|1(\omega t)\rangle$, will nominally become the new stationary state because $\mathrm{Re}\lambda_1 > \mathrm{Re}\lambda_0$. When this happens, the errors which are small in terms of the parameter $\|\omega\|/\|\lambda\|$, will receive a relative weight due to an exponential prefactor, here $e^{\int_0^\tau dt[\lambda_{1,t}-\lambda_{0,t}]}$, which grows exponentially large over time. This makes the adiabatic vector transport unstable. Moreover, if we perform the same expansion right from the start in a decaying mode, say $|1(\chi = 0)\rangle$, the same problem occurs even for a trivial spectrum, since all but the stationary mode are being exponentially suppressed. Due to this exponential growth, we should not think of Eq. (39) as an actual approximation of G_{ij} for small driving frequency ω, but rather as a formal expansion in the parameter $\|\omega\|/\|\lambda\|$, without making any statement about whether the higher orders are negligible or not.

Importantly, this does not hinder us from extracting the geometric phases through Eq. (39). The way out has implicitly already been mentioned before. Namely, as we stated already, through Eq. (38), we already have the full information of the individual λ_n at each t at our disposal. As a consequence, when computing G_{ij} for a time-dependent counting field, $\chi = \omega t$, it is possible to filter out at any time t any specific band n, by identifying it through its decay with $\lambda_n(t)$. Therefore, the same principle that is used to identify individual contributions of the single modes, serves at the same time to correct for unwanted transitions between bands. Once more, we will show how this is done in practice at the specific example which follows now.

2. *Practical example*

Now, we want to elaborate on how these recipes can be implemented at a specific practical example of a quantum point contact (QPC). We also briefly show the extent to which the observation of the fractional charges, and the corresponding geometric phases, are stable with respect measurement errors and detector backaction.

For the sake of concreteness, we consider again the simple single-level quantum dot model from Sec. II C, adding an explicit detector scheme. Since we believe that an actual measurement of electrons leaving or entering the right lead could be experimentally challenging, we propose to use a highly simplified measurement setup with a QPC capacitively coupled to the quantum dot, see Fig. 8(a), as it has been deployed in Ref. [57]. The current flowing through the QPC is sensitive to the charge state of the quantum dot, see Fig. 8(b). In the chosen example, the QPC has per se no direct means to distinguish the direction in which an electron tunnels. However, we can consider a regime where the chemical potentials are biased such that the charging and decharging events can with very high probability be associated to a charge transfer from the left, and to the right, respectively. To evaluate the transport statistics to the right, we can thus discard the charging events monitored by the QPC and only record the decharging events [as shown in Fig. 8(b)]. In this way, the detector will miss the very unlikely events of thermal excitation of electrons against the bias, which thus represents a first (small) source of measurement errors.

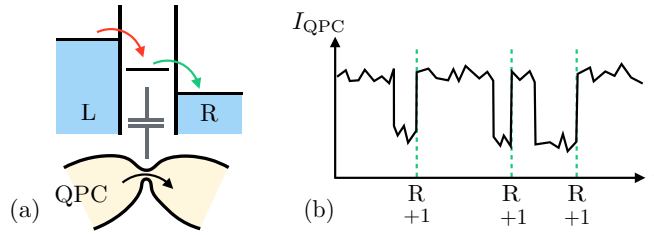

FIG. 8. (a) Measurement scheme to read-out the FCS of a single-level quantum dot. A quantum point contact (QPC) is capacitively coupled to the dot to time-dependently resolve the charge state. We assume a setup in which the chemical potentials are biased such that an electron entering the dot comes most likely from the left reservoir, whereas the electron leaves most likely to the right. (b) The current in the QPC as a function of time. Depending on the charge state on the quantum dot, the current is either reduced (filled dot) or not (empty). Since we are interested in the transport statistics into the right lead, we discard the charging events, and only record the decharging events. That is, each time the QPC current rises, we increase the detector state by one (indicated with the green, dashed line).

Consequently, the kernel defined in Eq. (10) has to be replaced by the new kernel

$$W_{\mathrm{QPC}}(\chi) = \sum_\alpha \begin{pmatrix} -2\Gamma_\alpha f_\alpha & \Gamma_\alpha[1-f_\alpha]e^{i\chi} \\ 2\Gamma_\alpha f_\alpha & -\Gamma_\alpha[1-f_\alpha] \end{pmatrix}, \tag{40}$$

that is, we measure the topology of W_{QPC} rather than W from Eq. (10). For the extreme limit $f_{\mathrm{L}} \to 1$ and $f_{\mathrm{R}} \to 0$, $W_{\mathrm{QPC}}(\chi)$ reduces to Eq. (10), thus, $W_{\mathrm{QPC}}(\chi)$ and $W(\chi)$ are equivalent. For finite thermal processes, the two differ slightly.

Along the lines of Sec. IV B, we can extract the eigenvalues $\lambda_n(\chi)$ of $W_{\mathrm{QPC}}(\chi)$ and the topology of the eigenspectrum through measuring the waiting-time distribution between two decharging events, $g_{++}(t)$. Since we have only the addition of charges to the right lead as a measured transport event, Eq. (38) simplifies to $g_{++}^{-1}(z) - e^{i\chi} = 0$, to determine $\lambda_n(\chi)$.

In addition, we may determine the geometric phase due to a parallel vector transport, as introduced previously in Sec. IV C. For this simple example, we now present the strategy to filter out a specific band, to avoid the adiabatic instability problem mentioned in Sec. IV C. To this end, we take the entire time interval τ, and discretize it, $\tau = \Delta t_0 + \Delta t_1 + \cdots + \Delta t_M$. For each time interval Δt_m, where m is integer and $0 \leqslant m \leqslant M$, we assign a constant counting field χ_m. This enables us to solve Eq. (37) piecewise exactly. We demonstrate the full derivation in Sec. S4 in the Supplemental Material [74]. Here we merely recapitulate the main steps. Note that we focus on G_{++}, since it is the only relevant correlator for the here considered detection scheme.

As it turns out, it is particularly useful to transform to Laplace space for each time interval. We define the operator for this transformation as $\mathcal{L}_M = \prod_{m=0}^{M} \int_0^\infty d\Delta t_m e^{-z\Delta t_m}$. This enables us to find a closed form for $G_{++}(z_0, z_1, \ldots) = \mathcal{L}_M G_{++}(\Delta t_0, \Delta t_1, \ldots)$. Now, the crucial step follows. We can compute the geometric phase

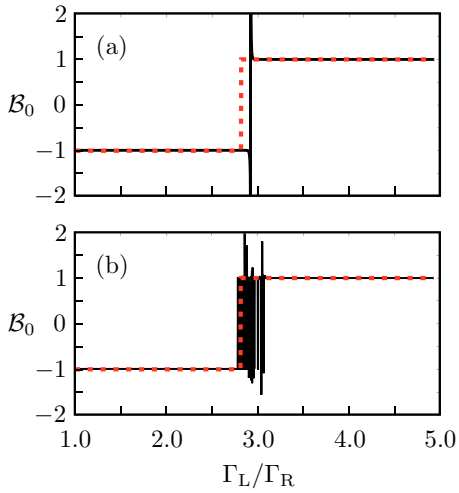

FIG. 9. The geometric phase $\mathcal{B}_0$ as a function of Γ_L/Γ_R for some error sources. The red dashed line corresponds to the exact $\mathcal{Z}$-number that would be expected for the quantum dot model if the measurement were ideal. In (a) the black curve corresponds to the case where an error occurs due the inaccurate measurement setup (see Fig. 8). Near the transition $\mathcal{B}_0$ becomes ill-defined. This is due to the numerical evaluation with finite elements, $\Delta\chi$. For $\Delta\chi$ approaching 0, the divergence dissappears, see also main text. In (b) we show (again in black) the curve due to fitting errors when extracting the parameters $g_{++,0}$, $g_{++,1}$ and l_0, l_1 from the waiting-time distribution. In general, we observe that while errors give rise to faulty behavior near the transition, the results are extremely stable away from the transition, thus allowing for a reliable measurement of topological numbers through waiting times. The parameters in both figures are $\mu_L - \epsilon = 5k_BT$, $\mu_R - \epsilon = -4k_BT$.

as $B_\nu = g_{++}^{-1}[\lambda_\nu(0)]\prod_{m=0}^{M}[z_m - \lambda_\nu(\chi_m)]G_{++}(z_0, z_1, \ldots)$ and subsequently take the limit of $z_m \to \lambda_\nu(\chi_m)$. In this way we filter out the contribution of the band of interest, ν, avoiding the instability occurring in the adiabatic time evolution. In the present example, we find that for $\nu = 0$ the geometric phase $\mathcal{B}_0 = e^{-\int_0^{2\pi p_0} d\chi \langle 0|\partial_\chi|0\rangle}$ is given as (see Sec. S4 in the Supplemental Material [74])

$$\mathcal{B}_0 = g_{++}^{-1}[\lambda_0(0)] \lim_{M\to\infty} \prod_{m=0}^{M-1} g_{++}[\lambda_0(\chi_m), \lambda_0(\chi_{m+1})] \times e^{i\chi_m} \frac{[\lambda_0(\chi_m) - l_0][\lambda_0(\chi_m) - l_1]}{\lambda_0(\chi_m) - \lambda_0(\chi_m + 2\pi)}, \tag{41}$$

with $\chi_m = 2\pi p_0 m/M$, and $g_{++}(z, z') = \sum_{n=0,1} g_{++,n}(z - l_n)^{-1}(z' - l_n)^{-1}$. Importantly, Eq. (41) explicitly shows that $\mathcal{B}_0$ can be expressed fully in terms of the function $g_{++}(z)$ and the eigenvalues $l_{0,1}$ of W_0, and is consequently directly accessible through the Laplace analysis of the waiting-time distribution.

In Fig. 9, we show the result of $\mathcal{B}_0$, as a function of Γ_L. That is, we assume that the experimenter can modify the tunnel coupling to at least one of the leads, and for each constellation of Γ_L/Γ_R, evaluates the waiting-time distribution of the detector. The red dashed line shows $\mathcal{B}_0$ for the original model given in Eq. (10), i.e., assuming ideal measurement. In Fig. 9(a), the black line corresponds to $\mathcal{B}_0$ for the simplified measurement scheme with the QPC, described in Eq. (40), and evaluated through the waiting-time distribution, according to Eq. (41). First, we observe that $\mathcal{B}_0$ evaluated through waiting times returns either ± 1. The fact that already $\mathcal{B}_0$ alone is quantized, and we do not need to take the product $\mathcal{Z} = \prod_\nu \mathcal{B}_\nu$, is due to the very simplified system with only two available states, and a detector only clicking in one direction (+). For a more complicated system, we would have to consider the product $\mathcal{Z}$ to obtain a quantized number. Note that very close to the transition, we find that $\mathcal{B}_0$ does not return ± 1, and instead becomes ill-defined. This is due to the fact, that the evaluation was done in a discretized way, with a finite resolution in χ, where M is finite. In the limit $M \to \infty$, the function approaches the exact step function. Second, we see that the transition from topological, $\mathcal{B}_0 = -1$, to trivial, $\mathcal{B}_0 = +1$, is shifted and occurs at a slightly different ratio of Γ_L/Γ_R. This is because the setup with the QPC is missing the thermally excited processes. Thus the detector overestimates the current, which renders the topological phase more stable (i.e., the system is in the topological phase for a larger parameter subspace). We can similarly expect that for another type of error, which underestimates the current, the effect would be the opposite, that is, a less stable topological phase.

Next, we comment on errors in the fitting process. Namely, we may imagine that for each setting of Γ_L/Γ_R, the experimenter performs a new evaluation of the detector dynamics, and fits the function $g_{++}(\tau)$ with a double exponential to extract the indices $g_{++,0}$, $g_{++,1}$ and l_0, l_1. It is then reasonable to assume that the fitting process might be subject to fluctuations for each setting. We here model these fluctuations as follows. We supplement the four extracted parameters, $g_{++,n}$ and l_n, each with an independent small error, $g_{++,n} + \delta g_{++,n}$ and $l_n + \delta l_n$, which we update with pseudorandom numbers for each value of Γ_L/Γ_R. In Fig. 9(b), we choose the error magnitude such that both δg_{++} and δl change within 10% of the original value g_{++} or l, respectively. We see that close to values of Γ_L/Γ_R where the transition occurs in the ideal case, the fluctuations lead to a random back and forth switching between $\mathcal{B}_0 = +1$ and -1. This is because in this critical region, a small change in the g_{++}'s and l's can undo, respectively, redo the braid phase transition. Far away from this region, the topological phases remain stable.

Finally, let us point out, that apart from small errors due to the specific measurement setup, there can also more systematic errors. As far as systematic errors are concerned, we have already commented on some aspects in Sec. II C. To repeat, in the quantum dot models we have dismissed levels and charge states that are beyond the resonant energy window. Due to small temperatures, these states are either mostly empty or mostly filled all the time, and therefore provide small corrections to the current. These small corrections manifest themselves in the spectrum of $W(\chi)$ as eigenvalues with only a very weak χ-dependence. They can therefore be considered as topologically inert eigenmodes, that do not partake in any braid phase transition, and lead at most to small corrections of the eigenspectrum. When accessing the detector dynamics through waiting times, such inert eigenvalues will appear as small corrections in the measured correlators $g_{ij}(\tau)$, and will likely remain undetected. To give an example, suppose that there are two important modes (just as in the single-level

quantum dot), and a potentially arbitrary number of modes with only weak χ-dependence. Then, $g_{ij}(\tau) = \sum_n g_{ij,n} e^{l_n \tau}$ will have two significant coefficients $g_{ij,0}$ and $g_{ij,1}$, and all other coefficients $|g_{ij,n\geqslant 2}| \ll |g_{ij,0}|, |g_{ij,1}|$.

Similarly, detector backaction does not pose a significant thread for the topology. Detector-induced dephasing [112] is obviously of no concern in the here studied purely classical dynamics. Apart from that, the QPC can induce inelastic transitions in the quantum system due to noise [113,114]. However, as long as these processes are improbable (which can be assured by appropriately tuning the QPC parameters [113]), they cannot pose any threat to the observation of the topological phases, as the latter are by definition stable with respect to small variations of the parameters. Furthermore, a finite reaction time of the QPC has been studied in Ref. [57], which is, however, at least one order of magnitude faster than the tunneling dynamics. This additional effect would give rise to additional modes which are decaying very fast. Due to this separation of timescale, such modes can likewise not partake in a braid phase transition (see again our discussion in Sec. II C).

Overall, we have examined backaction as well as some realistic errors due to the concrete measurement setup, none of which can destroy the braid phase transition in the eigenspectrum, nor hinder the observation of the associated geometric phase $\mathcal{B}$. As we showed at some examples, errors merely meddle with the precise measurement of the location where the topological transition appears. We further note, that in the examples above, we went to rather high error amplitudes, to render the effects visible in Fig. 9. In reality, we are confident that those errors can be reduced significantly.

In fact, let us note at this point that in Ref. [57] the waiting-time distribution of a quantum dot coupled to a QPC has indeed been experimentally measured. Their setup thus would allow for the extraction of this quantized phase. Unfortunately, the raw data of the waiting-time distribution is not available from Ref. [57], which is why we cannot directly extract the geometric phases $\mathcal{B}_n$ and their product $\mathcal{Z}$. However, considering the values of the tunneling rates they extract, they find the ratio $\Gamma_L/\Gamma_R = 0.25$. Thus, their system should actually be in the topological phase with $e_0^* = e/2$ and $\mathcal{Z} = -1$. To observe a transition from topological to trivial, the waiting times would have to be extracted for different ratios of Γ_L and Γ_R, which was not done in Ref. [57].

D. Going beyond the resolution limit

As we have argued in Sec. II D, we can directly link the mismatch between fractional charges and integer charge quantization, and the resulting periodicity breaking due to a braid phase transition, to a detector measuring a discrete process below its resolution limit. We expect that the latter provides new applications for measuring techniques. To demonstrate this principle at work, we consider a very straightforward extension of the previously introduced simple QPC setup (see Fig. 8). Namely, we can add a second level to the system, where for simplicity, we consider two extreme cases. We either consider again the serial double quantum dot model from Fig. 4 with a QPC, which is now coupled equally to both islands; see Fig. 10(a). This corresponds to an archetype example of a detector that cannot resolve the two individual islands.

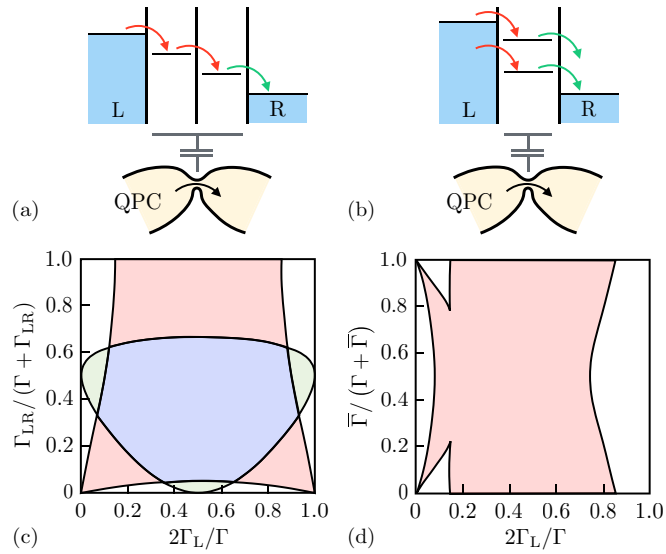

FIG. 10. Transport models to illustrate the principle of resolving processes beyond the detector's resolution limit. The electrons may tunnel through two levels in either a serial (a) or a parallel (b) configuration. The statistics are measured through a QPC which cannot resolve individual charge islands. In (c) and (d) we show the topological phase diagram for the serial and parallel configuration, respectively, as a function of the tunnel coupling parameters. We defined $\Gamma = 2\Gamma_L + \Gamma_R$ and $\overline{\Gamma} = 2\overline{\Gamma}_L + \overline{\Gamma}_R$. On the x axis of both figures, we change the left and right asymmetry, $2\Gamma_L/\Gamma$, where for (d) we assume for simplicity $2\Gamma_L/\Gamma = 2\overline{\Gamma}_L/\overline{\Gamma}$. On the y axis of (c) we modify the relative tunneling rate of the inelastic process, $\Gamma_{in}/(\Gamma + \Gamma_{in})$, whereas in (d) we modify the relative total tunneling rate for each level, $\overline{\Gamma}/(\Gamma + \overline{\Gamma})$. In (c) and (d) the white areas correspond to a fully trivial eigenspectrum of $W(\chi)$. The red area corresponds to the same topological phase as in Fig. 4(c), with a braided stationary mode with a fractional charge $e_0^* = e/2$. The blue and green areas indicate the topological phases as shown in Figs. 4(b) and 4(d), respectively, and occur only in the serial level configuration. In particular, the blue phase, where all three eigenvalues merge to a band with charge $e_0^* = e/3$, is stable for a large parameter space, and provides a unique signature of the presence of two serially coupled islands instead of one.

We put this system into relation with another one, containing only one charge island (a SQD), however, with *two* available levels instead of one. Importantly, note that if we were to compare the serial DQD to a SQD with only one available level, as in Fig. 2, we would not need any sophisticated topological argument to differentiate the two systems, as we could already infer the presence of the second dot simply by counting the number of degrees of freedom in the waiting-time distribution: in the SQD, we have only two dominant eigenvalues, whereas in the DQD we have three. The distinction between a single and a double island, however, is less straightforward, if the single island has two levels, which are not coupled in series, but in parallel; see Fig. 10(b). Here, both systems have three dominant eigenmodes. We tune yet again the energy levels and charging energies, such that only one extra electron can enter the quantum system, and

electron transport goes with very high probability towards the right. Once more, we neglect any spurious thermal errors, i.e., thermally excited processes going against the energy gradient (as the topology is stable with respect to such small errors). As a consequence, we can write the kernel of the serial model simply as

$$W_{\mathrm{s}}(\chi) = \begin{pmatrix} -2\Gamma_{\mathrm{L}} & 0 & \Gamma_{\mathrm{R}} e^{i\chi} \\ 2\Gamma_{\mathrm{L}} & -\Gamma_{\mathrm{LR}} & 0 \\ 0 & \Gamma_{\mathrm{LR}} & -\Gamma_{\mathrm{R}} \end{pmatrix}, \tag{42}$$

where the factor $e^{i\chi}$ takes again into account that we only record the decharging events in I_{QPC}. As for the parallel configuration, we find

$$W_{\mathrm{p}}(\chi) = \begin{pmatrix} -2\Gamma_{\mathrm{L}} - 2\overline{\Gamma}_{\mathrm{L}} & \Gamma_{\mathrm{R}} e^{i\chi} & \overline{\Gamma}_{\mathrm{R}} e^{i\chi} \\ 2\Gamma_{\mathrm{L}} & -\Gamma_{\mathrm{R}} & 0 \\ 2\overline{\Gamma}_{\mathrm{L}} & 0 & -\overline{\Gamma}_{\mathrm{R}} \end{pmatrix}, \tag{43}$$

where the third row (column) account for the coupling with the second level at higher energies, which are coupled through the rates $\overline{\Gamma}_{\mathrm{L}}, \overline{\Gamma}_{\mathrm{R}}$.

Crucially, while the two systems cannot be distinguished by the number of degrees of freedom, they can be distinguished based on the topology of the QPC dynamics. In fact, the topological phases that occur in the serial configuration were analyzed already in Sec. II C. In Fig. 10(c), we show the phase diagram as a function of the tunnel coupling rates. In particular, there is a very stable phase with three braided eigenvalues (blue area) for a large parameter space, with a spectrum of periodicity $p_0 = 3$ and thus the charge $e/3$, see also Fig. 4(b). Through making the tunneling rates more and more asymmetric, the system-detector dynamics changes to the simpler braid topology with a spectrum as in Figs. 4(c) and 4(d) (red and green areas, respectively), and finally to a trivial phase (white area).

Importantly, the $e/3$ phase occurs exclusively in the serial configuration. In the parallel configuration, see Fig. 10(d), the QPC dynamics are either trivial (white area) or have a braided stationary mode with charge $e_0^* = e/2$ (red area). No other topological phases can be observed in spite of the presence of a second available level. The reason for the absence of the $e/3$ phase can be explained intuitively, when representing the processes in a graph including the detector states N; see Fig. 11. While the serial DQD can be represented as a process with a step size three times smaller than the detector resolution [Fig. 11(a)], the same cannot be accomplished in the parallel configuration. For the latter, there are only two consecutive processes needed to move to the next detector pixel [Fig. 11(b)]. We conclude that the occurrence of the $e/3$ phase is a direct consequence of the fact that in the serial configuration an electron needs to execute three consecutive tunneling events. Thus, we find a unique topological signature in the statistics of a QPC detector, which enables us to determine the presence or absence of a second charge island for a large parameter regime, even if the detector cannot distinguish the islands. As we have already shown in the previous section, small errors and deviations from the ideal models considered here, cannot destroy the effect.

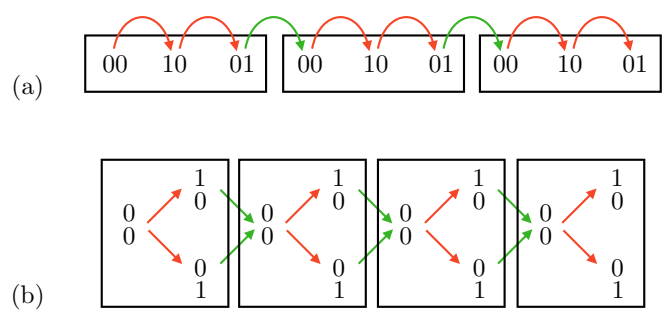

FIG. 11. Representation of the system-detector dynamics of the transport through a serial (a) and a parallel (b) level configuration. The black rectangles represent the detector pixels. Only processes that change between different pixels are the ones registered by the QPC (green arrows), the others are undetected (red arrows). In the serial configuration (a) in each pixel, there are three available states, either both quantum dots empty (00), or one electron in the left (10) or the right dot (01). To move to the next pixel, we need to perform three consecutive tunneling events. While in the parallel configuration (b) there are likewise three states within one pixel (either both levels empty, or either the lower or the upper level filled with one electron), one needs only two consecutive processes to change the detector pixel. Therefore, the $e/3$ phase is impossible in the latter case.

Finally, we anticipate that the braid topology could potentially be useful well beyond the context of quantum transport, as a general tool to observe the dynamics of very small, discrete processes beyond the detector's resolution limit. In the example above, and in Sec. II D, we have so far focused on the limit of a detector resolution which is commensurable with the step size of the discrete process. In the general discussion in Sec. II D, this fact was expressed in the detector resolution $\mathcal{A}$ being an integer multiple of e^*. In the concrete example here, we have considered one QPC which measures two dots (or charge islands). To generalize this idea, we believe it is of very high interest to include the possibility of a detector resolution $\mathcal{A}$ that is incommensurable with the step size of the observed discrete process. This question goes, however, well beyond the scope of the present work and will be pursued in the future.

V. CONCLUSION

In this work, we have shown that a topological transition in the system-detector dynamics leads to FCS with eigenmodes carrying fractional charges. This realization relies on the fact that the fundamental integer charge quantization fixes the global properties of the moment generating function, and on the proposition that fractional charges can only be well-defined by means of an analytic continuation of the eigenmodes of the moment generating function. In particular, we showed that we can map the dynamics of topological FCS in a very generic transport situation to a hypothetical system with fractionally charged quasiparticles, supplemented with a charge detector with integer charge resolution, ensuring the indivisibility of the elementary charge. Our result therefore raises the question how far the transport

signatures of fractionally charged quasiparticles are unique to exotic excitations, such as Luttinger liquid or Laughlin quasiparticles.

We have further demonstrated the existence of a generalized geometric phase, which gives rise to a topological number directly indicating the mismatch between fractional charges and integer charge quantization. Moreover, we have shown that this topological number allows us to establish a profound analogy to the topology of the fractional Josephson effect in superconducting junctions, thus comparing a system with fully dissipative transport to a system with coherent supercurrents. This provides an unexpected possibility to simulate crucial aspects of the transport physics of strongly correlated quantum systems by means of classical, incoherent dynamics.

We have provided explicit strategies to verify the various claims in experiments. First, we have identified a regime of nearly Poissonian statistics of fractional charges, which can be measured through low cumulants. Beyond the effectively Poissonian regime, we have shown how to extract the fractional charges and the geometric phase from the waiting-time distribution. Thus, we potentially open up a new road to characterise the topology of open quantum systems by means of the detector degree of freedom. An important future project could aim at generalizing this concept to multidimensional systems, where more than one quantity is measured. Finally, we have shown at a simple, easily realizable example, that the fractional effect can be used to detect the presence of multiple charge islands even when the charge detector cannot distinguish them directly. This could open up a new research direction to use topological effects in the detector dynamics for novel measurement techniques. In future research, this effect could potentially be extended to cases when the resolution of the discrete process and the detector resolution are incommensurate.

ACKNOWLEDGMENTS

The author is greatly indepted to Janine Splettstoesser and to Maarten Wegewijs who provided invaluable advice on many of the here treated topics, and for many highly stimulating discussions. A thank you for very helpful and interesting discussions goes also to Thomas L. Schmidt, Sebastian Diehl, Jakob V. Schwibbert, Gianluigi Catelani, Björn Sothmann, and Philipp Stegmann. This work has been funded by the German Federal Ministry of Education and Research within the funding program Photonic Research Germany under the Contract No. 13N14891.

[1] R. B. Laughlin, Phys. Rev. Lett. **50**, 1395 (1983).
[2] J. Alicea and P. Fendley, Annu. Rev. Condens. Matter Phys. **7**, 119 (2016).
[3] K.-V. Pham, M. Gabay, and P. Lederer, Phys. Rev. B **61**, 16397 (2000).
[4] B. Trauzettel, I. Safi, F. Dolcini, and H. Grabert, Phys. Rev. Lett. **92**, 226405 (2004).
[5] H. Steinberg, G. Barak, A. Yacoby, L. N. Pfeiffer, K. W. West, B. I. Halperin, and K. Le Hur, Nat. Phys. **4**, 116 (2007).
[6] S. Das Sarma, M. Freedman, and C. Nayak, Phys. Rev. Lett. **94**, 166802 (2005).
[7] L. Saminadayar, D. C. Glattli, Y. Jin, and B. Etienne, Phys. Rev. Lett. **79**, 2526 (1997).
[8] R. de Picciotto, M. Reznikov, M. Heiblum, V. Umansky, G. Bunin, and D. Mahalu, Nature **389**, 162 (1997).
[9] M. Reznikov, R. d. Picciotto, T. G. Griffiths, M. Heiblum, and V. Umansky, Nature **399**, 238 (1999).
[10] E. Comforti, Y. C. Chung, M. Heiblum, V. Umansky, and D. Mahalu, Nature **416**, 515 (2002).
[11] M. Dolev, M. Heiblum, V. Umansky, A. Stern, and D. Mahalu, Nature **452**, 829 (2008).
[12] D. C. Glattli and P. S. Roulleau, Phys. Status Solidi B **254**, 1600650 (2017).
[13] M. Kapfer, P. Roulleau, M. Santin, I. Farrer, D. A. Ritchie, and D. C. Glattli, Science **363**, 846 (2019).
[14] D. B. Gutman, Y. Gefen, and A. D. Mirlin, Phys. Rev. Lett. **105**, 256802 (2010).
[15] Y. V. Nazarov and Y. M. Blanter, *Quantum Transport: Introduction to Nanoscience* (Cambridge University Press, Cambridge, 2009).
[16] J. Ren and N. A. Sinitsyn, Phys. Rev. E **87**, 050101(R) (2013).
[17] F. Li, J. Ren, and N. A. Sinitsyn, Europhys. Lett. **105**, 27001 (2014).
[18] X. G. Wen, Phys. Rev. B **41**, 12838 (1990).
[19] C. L. Kane and M. P. A. Fisher, Phys. Rev. Lett. **72**, 724 (1994).
[20] T. Jonckheere, M. Creux, and T. Martin, Phys. Rev. B **72**, 205321 (2005).
[21] J. Keeling, I. Klich, and L. S. Levitov, Phys. Rev. Lett. **97**, 116403 (2006).
[22] F. Pistolesi, Phys. Rev. B **69**, 245409 (2004).
[23] A. Croy and U. Saalmann, Phys. Rev. B **93**, 165428 (2016).
[24] M. Moskalets, Phys. Rev. Lett. **117**, 046801 (2016).
[25] M. Hasegawa, Étienne Jussiau, and R. S. Whitney, Phys. Rev. B **100**, 125420 (2019).
[26] M. Z. Hasan and C. L. Kane, Rev. Mod. Phys. **82**, 3045 (2010).
[27] C.-K. Chiu, J. C. Y. Teo, A. P. Schnyder, and S. Ryu, Rev. Mod. Phys. **88**, 035005 (2016).
[28] C.-E. Bardyn, M. A. Baranov, C. V. Kraus, E. Rico, A. Imamoglu, P. Zoller, and S. Diehl, New J. Phys. **15**, 085001 (2013).
[29] J. C. Budich and S. Diehl, Phys. Rev. B **91**, 165140 (2015).
[30] T. Pluecker, M. R. Wegewijs, and J. Splettstoesser, Phys. Rev. B **95**, 155431 (2017).
[31] T. Pluecker, M. R. Wegewijs, and J. Splettstoesser, arXiv:1711.10431v1.
[32] D. Leykam, K. Y. Bliokh, C. Huang, Y. D. Chong, and F. Nori, Phys. Rev. Lett. **118**, 040401 (2017).
[33] F. K. Kunst, E. Edvardsson, J. C. Budich, and E. J. Bergholtz, Phys. Rev. Lett. **121**, 026808 (2018).
[34] C.-E. Bardyn, L. Wawer, A. Altland, M. Fleischhauer, and S. Diehl, Phys. Rev. X **8**, 011035 (2018).
[35] S. Yao and Z. Wang, Phys. Rev. Lett. **121**, 086803 (2018).

[36] E. Edvardsson, F. K. Kunst, and E. J. Bergholtz, Phys. Rev. B **99**, 081302(R) (2019).

[37] L. Fu and C. L. Kane, Phys. Rev. B **79**, 161408(R) (2009).

[38] E. Bocquillon, R. S. Deacon, J. Wiedenmann, P. Leubner, T. M. Klapwijk, C. Brüne, K. Ishibashi, H. Buhmann, and L. W. Molenkamp, Nat. Nanotechnol. **12**, 137 (2016).

[39] J. Wiedenmann, E. Bocquillon, R. S. Deacon, S. Hartinger, O. Herrmann, T. M. Klapwijk, L. Maier, C. Ames, C. Brüne, C. Gould, A. Oiwa, K. Ishibashi, S. Tarucha, H. Buhmann, and L. W. Molenkamp, Nat. Commun. **7**, 10303 (2016).

[40] R. S. Deacon, J. Wiedenmann, E. Bocquillon, F. Domínguez, T. M. Klapwijk, P. Leubner, C. Brüne, E. M. Hankiewicz, S. Tarucha, K. Ishibashi, H. Buhmann, and L. W. Molenkamp, Phys. Rev. X **7**, 021011 (2017).

[41] F. Zhang and C. L. Kane, Phys. Rev. Lett. **113**, 036401 (2014).

[42] C. P. Orth, R. P. Tiwari, T. Meng, and T. L. Schmidt, Phys. Rev. B **91**, 081406(R) (2015).

[43] Y. Vinkler-Aviv, P. W. Brouwer, and F. von Oppen, Phys. Rev. B **96**, 195421 (2017).

[44] A. Souslov, B. C. van Zuiden, D. Bartolo, and V. Vitelli, Nat. Phys. **13**, 1091 (2017).

[45] H. Abbaszadeh, A. Souslov, J. Paulose, H. Schomerus, and V. Vitelli, Phys. Rev. Lett. **119**, 195502 (2017).

[46] G. Engelhardt, M. Benito, G. Platero, G. Schaller, and T. Brandes, Phys. Rev. B **96**, 241404(R) (2017).

[47] B. van Heck, F. Hassler, A. R. Akhmerov, and C. W. J. Beenakker, Phys. Rev. B **84**, 180502(R) (2011).

[48] D. Rainis and D. Loss, Phys. Rev. B **85**, 174533 (2012).

[49] B. Reulet, J. Senzier, and D. E. Prober, Phys. Rev. Lett. **91**, 196601 (2003).

[50] Y. Bomze, G. Gershon, D. Shovkun, L. S. Levitov, and M. Reznikov, Phys. Rev. Lett. **95**, 176601 (2005).

[51] S. Gustavsson, R. Leturcq, B. Simovič, R. Schleser, T. Ihn, P. Studerus, K. Ensslin, D. C. Driscoll, and A. C. Gossard, Phys. Rev. Lett. **96**, 076605 (2006).

[52] T. Fujisawa, Science **312**, 1634 (2006).

[53] A. V. Timofeev, M. Meschke, J. T. Peltonen, T. T. Heikkilä, and J. P. Pekola, Phys. Rev. Lett. **98**, 207001 (2007).

[54] E. V. Sukhorukov, A. N. Jordan, S. Gustavsson, R. Leturcq, T. Ihn, and K. Ensslin, Nat. Phys. **3**, 243 (2007).

[55] G. Gershon, Y. Bomze, E. V. Sukhorukov, and M. Reznikov, Phys. Rev. Lett. **101**, 016803 (2008).

[56] Q. Le Masne, H. Pothier, N. O. Birge, C. Urbina, and D. Esteve, Phys. Rev. Lett. **102**, 067002 (2009).

[57] C. Flindt, C. Fricke, F. Hohls, T. Novotný, K. Netočný, T. Brandes, and R. J. Haug, Proc. Natl. Acad. Sci. USA **106**, 10116 (2009).

[58] N. Ubbelohde, C. Fricke, C. Flindt, F. Hohls, and R. J. Haug, Nat. Commun. **3**, 612 (2012).

[59] K. Brandner, V. F. Maisi, J. P. Pekola, J. P. Garrahan, and C. Flindt, Phys. Rev. Lett. **118**, 180601 (2017).

[60] J. Koch, M. E. Raikh, and F. von Oppen, Phys. Rev. Lett. **95**, 056801 (2005).

[61] T. Brandes, Ann. Phys. **17**, 477 (2008).

[62] S. Welack, S. Mukamel, and Y. Yan, Europhys. Lett. **85**, 57008 (2009).

[63] M. Albert, C. Flindt, and M. Büttiker, Phys. Rev. Lett. **107**, 086805 (2011).

[64] L. Rajabi, C. Pöltl, and M. Governale, Phys. Rev. Lett. **111**, 067002 (2013).

[65] B. Sothmann, Phys. Rev. B **90**, 155315 (2014).

[66] E. Potanina and C. Flindt, Phys. Rev. B **96**, 045420 (2017).

[67] X. Jehl, M. Sanquer, R. Calemczuk, and D. Mailly, Nature **405**, 50 (2000).

[68] L. A. Landau, E. Cornfeld, and E. Sela, Phys. Rev. Lett. **120**, 186801 (2018).

[69] F. D. M. Haldane, J. Phys. C: Solid State Phys. **14**, 2585 (1981).

[70] C. Flindt and J. P. Garrahan, Phys. Rev. Lett. **110**, 050601 (2013).

[71] J. M. Hickey, C. Flindt, and J. P. Garrahan, Phys. Rev. E **90**, 062128 (2014).

[72] A. Imambekov, T. L. Schmidt, and L. I. Glazman, Rev. Mod. Phys. **84**, 1253 (2012).

[73] T. L. Schmidt (private communications).

[74] See Supplemental Material at http://link.aps.org/supplemental/10.1103/PhysRevB.100.245416 for details on several proofs and derivations.

[75] J. Splettstoesser, M. Governale, J. König, and M. Büttiker, Phys. Rev. B **81**, 165318 (2010).

[76] L. D. Contreras-Pulido, J. Splettstoesser, M. Governale, J. König, and M. Büttiker, Phys. Rev. B **85**, 075301 (2012).

[77] R. B. Saptsov and M. R. Wegewijs, Phys. Rev. B **86**, 235432 (2012).

[78] R. B. Saptsov and M. R. Wegewijs, Phys. Rev. B **90**, 045407 (2014).

[79] J. Schulenborg, J. Splettstoesser, M. Governale, and L. D. Contreras-Pulido, Phys. Rev. B **89**, 195305 (2014).

[80] L. S. Levitov, H. Lee, and G. B. Lesovik, J. Math. Phys. **37**, 4845 (1996).

[81] G. Schaller, G. Kießlich, and T. Brandes, Phys. Rev. B **80**, 245107 (2009).

[82] Y. V. Nazarov and D. A. Bagrets, Phys. Rev. Lett. **88**, 196801 (2002).

[83] D. A. Bagrets and Y. V. Nazarov, Phys. Rev. B **67**, 085316 (2003).

[84] E. Artin, Ann. Math. **48**, 101 (1947).

[85] In analogy to bands in solid state physics, where here, χ resumes a similar role as the k vector in the Hamiltonian description of a crystal, i.e., a detector momentum.

[86] J. König, Quantum fluctuations in the single-electron transistor, Ph.D. thesis, University of Karlsruhe, Germany, 1999.

[87] W. Belzig, Phys. Rev. B **71**, 161301(R) (2005).

[88] D. Andrieux and P. Gaspard, J. Stat. Mech.: Theory Exp. (2007) P02006.

[89] M. Esposito, U. Harbola, and S. Mukamel, Rev. Mod. Phys. **81**, 1665 (2009).

[90] T. Fujisawa, T. H. Oosterkamp, W. G. van der Wiel, B. W. Broer, R. Aguado, S. Tarucha, and L. P. Kouwenhoven, Science **282**, 932 (1998).

[91] X. Hu, B. Koiller, and S. Das Sarma, Phys. Rev. B **71**, 235332 (2005).

[92] B. Roche, R.-P. Riwar, B. Voisin, E. Dupont-Ferrier, R. Wacquez, M. Vinet, M. Sanquer, J. Splettstoesser, and X. Jehl, Nat. Commun. **4**, 1581 (2013).

[93] N. A. Sinitsyn and I. Nemenman, Europhys. Lett. **77**, 58001 (2007).

[94] N. A. Sinitsyn and I. Nemenman, Phys. Rev. Lett. **99**, 220408 (2007).

[95] N. A. Sinitsyn, J. Phys. A: Math. Theor. **42**, 193001 (2009).

[96] J. Ren, P. Hänggi, and B. Li, Phys. Rev. Lett. **104**, 170601 (2010).
[97] S. Diehl, E. Rico, M. A. Baranov, and P. Zoller, Nat. Phys. **7**, 971 (2011).
[98] There is an exception: In a general matrix with the property $W^*(\chi) = W(-\chi)$ there can in principle occur pairs of eigenvalues with $\lambda^*_{\nu_1}(\chi) = \lambda_{\nu_2}(-\chi)$. Here, the individual geometric phases of either ν_1 or ν_2 are not guaranteed to be real. The product of the geometric phases, however, still is. In the example systems where we study the geometric phase explicitly, we do not encounter such a case, which is why we do not discuss this in detail.
[99] R.-P. Riwar, M. Houzet, J. S. Meyer, and Y. V. Nazarov, Nat. Commun. **7**, 11167 (2016).
[100] C. Z. Ning and H. Haken, Mod. Phys. Lett. B **06**, 1541 (1992).
[101] A. S. Landsberg, Phys. Rev. Lett. **69**, 865 (1992).
[102] J. Alicea, Y. Oreg, G. Refael, F. von Oppen, and M. P. A. Fisher, Nat. Phys. **7**, 412 (2011).
[103] C. W. J. Beenakker, Phys. Rev. Lett. **67**, 3836 (1991).
[104] Let us mention that for the open circuit, the QSHI brought for by Ref. [37] might strictly speaking not be the right choice of material, since we cannot open the loop without coupling the edge states on either side of the sample. We note, however, that many other realizations of Kitaev chains do not suffer from this restriction, such as the proposal in Ref. [102].
[105] Y. Song and S. Das Sarma, Phys. Rev. B **98**, 075159 (2018).
[106] X. You, J. A. Sauls, and J. Koch, Phys. Rev. B **99**, 174512 (2019).
[107] A. Thielmann, M. H. Hettler, J. König, and G. Schön, Phys. Rev. B **68**, 115105 (2003).
[108] A. Deger, K. Brandner, and C. Flindt, Phys. Rev. E **97**, 012115 (2018).
[109] P. Stegmann and J. König, New J. Phys. **19**, 023018 (2017).
[110] A. Mostafazadeh, Phys. Rev. A **55**, 1653 (1997).
[111] A. Bednorz and W. Belzig, Phys. Rev. Lett. **101**, 206803 (2008).
[112] E. Buks, R. Schuster, M. Heiblum, D. Mahalu, and V. Umansky, Nature **391**, 871 (1998).
[113] E. Onac, F. Balestro, L. H. Willems van Beveren, U. Hartmann, Y. V. Nazarov, and L. P. Kouwenhoven, Phys. Rev. Lett. **96**, 176601 (2006).
[114] S. Gustavsson, M. Studer, R. Leturcq, T. Ihn, K. Ensslin, D. C. Driscoll, and A. C. Gossard, Phys. Rev. Lett. **99**, 206804 (2007).